J. metamorphic Geol., 1992, 10, 651–669

Blue amphiboles and their significance for the metamorphic history of the Pan-African Gariep belt, Namibia

H. E. FRIMMEL AND C. J. H. HARTNADY
Precambrian Research Unit, Department of Geology, University of Cape Town, Rondebosch 7700, South Africa

ABSTRACT The metamorphic history of mafic exotic blocks from a tectonic melange zone within an allochthonous ophiolitic terrane (Marmora Terrane) of the Pan-African Gariep orogenic belt in south-western Namibia was studied, based on mineral parageneses and amphibole composition. Glaucophane described previously from these rocks could not be verified. Instead, two types of blue amphiboles were distinguished: (i) rims of (ferro-) edenitic to pargasitic to barroisitic hornblende composition around brownish amphibole phenocrysts replacing magmatic clinopyroxene, and (ii) deep blue porphyroblasts of magnesio-riebeckite with little ferro-glaucophane component in a highly metasomatized albite-rich rock. Textural and mineralogical evidence, particularly the existence of up to three different amphibole generations in metagabbro samples, supports a multiphase metamorphic history experienced by these exotic blocks. The first metamorphic event, M1, is interpreted as very low-P hydrothermal oceanic metamorphism that affected the igneous protoliths at up to amphibolite facies temperatures. Subsequent M2 metamorphism was syntectonic and is characterized by temperatures similar to those attained during M1 but higher pressures indicating burial to 15–20 km. This event is related to a subduction process. The third metamorphic event, M3, was low grade and of regional nature. It is the only one recorded in the sedimentary envelope of the exotic blocks. The formation of magnesio-riebeckite is considered a retrograde reaction at greenschist facies during M2. The results indicate that in the Gariep belt subduction and subsequent obduction have occurred, although blueschist facies metamorphism has not been reached.

Key words: blueschist facies metamorphism; Gariep orogenic belt, Namibia; magnesio-riebeckite.

INTRODUCTION

The late Proterozoic–early Palaeozoic Gariep belt forms part of the Pan-African belts of equatorial and southern Africa. Tectonic models for these belts are mainly based on the probably best-studied Pan-African orogenic feature of the area, the Damara orogen. The term 'Damara orogen' (*sensu lato*) usually refers to a diverging structure consisting of two branches: (i) a coastal branch, the Kaoko belt, extending northwards to join the West Congolian belt; and (ii) an intracontinental branch, the Damara belt *sensu stricto*, that can be connected in the north-east with the Lufilian Arc and the Zambezi belt in Zambia, and in the south with the Gariep belt and the Saldania belt in southern Namibia and South Africa (Martin & Porada, 1977; Porada, 1989). Much of the coastal branches, like the Gariep and the Kaoko belts, is not accessible due to the later opening of the South Atlantic. The equivalent to the Damara orogen (*s.l.*) on the other side of the South Atlantic is seen in the Ribeira belt of Brazil and Uruguay (see Fig. 1; Porada, 1979).

Various models have been proposed for the evolution of the Damara orogen which differ essentially in the assumed width, or existence at all, respectively, of oceanic crust between the Congo and the Kalahari cratons: (i) an orogen–aulacogen model with a triple junction of continental rifts, formed above an uprising mantle plume west of the present coast of Namibia (Martin & Porada, 1977; Porada, 1979); (ii) a Wilson-cycle model with sea-floor spreading, subduction and subsequent continental collision (Barnes & Sawyer, 1980; Kasch, 1983b; Miller, 1983); and (iii) a propagating rift model with the progressive opening of the proto-South Atlantic from the Gariep belt towards the north and then north-eastwards into the continent (Porada, 1983, 1989).

The application of a modern Wilson-cycle model to the Damara orogen (*s.l.*) is inhibited by only equivocal evidence of oceanic crust and the lack of blueschist and/or eclogite facies metamorphism (Miller, 1983). However, an increased P/T ratio during synorogenic metamorphism is recorded in metapelitic rocks in the Southern Zone of the intracontinental branch (Kasch, 1983a). The only area where plate tectonic processes similar to a modern Wilson-cycle model are believed to be documented is in the relatively poorly studied Gariep belt along the coastal region of south-western Namibia and north-western South

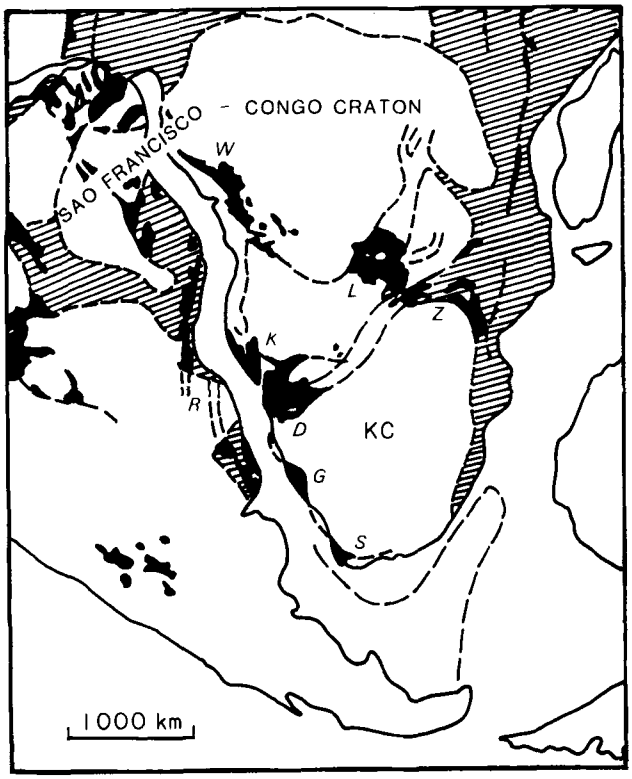

Fig. 1. The Gariep belt (G) in the framework of Pan-Gondwana orogenic belts in western Africa and eastern South America (modified after Porada, 1989): KC = Kalahari craton, D = Damara belt, K = Kaoko belt, L = Lufilian Arc, R = Ribeira belt, S = Saldania belt, W = West Congolian belt, Z = Zambezi belt.

Africa. There, mafic and ultramafic bodies in the Marmora Terrane (Hartnady *et al.*, 1990) are considered to represent obducted ophiolites. Their geochemical characteristics and tectonic setting are currently being studied and will be presented elsewhere.

One of the most compelling arguments for a major plate collision event is based on 'glaucophane-bearing schists' reported from the Gariep belt (Porada, 1989). Glaucophanitic amphiboles were mentioned by Kaiser as early as 1926, and later by Kröner (1974), but no detailed study of these amphiboles was carried out despite their significance for the tectonic evolution of the Gariep belt in particular, and plate tectonic processes during Pan-Gondwana orogeny in general.

In this paper we present electron microprobe (EMP) data of 'blue amphiboles' and associated minerals constituting exotic mafic blocks that were found in a tectonic melange zone in the western, allochthonous part of the Gariep belt. The petrogenetic implications of the mineral assemblages determined and particularly those of compositional variation of amphiboles in metamorphosed basalts and gabbros are discussed.

GEOLOGICAL SETTING AND MODE OF OCCURRENCE

The Gariep belt consists of an eastern para-autochthonous passive continental margin zone, the Port Nolloth zone, and a western allochthonous ophiolitic terrane, the Marmora Terrane, juxtaposed at the Schakalsberge Thrust (Fig. 2). From south-east to north-west, the Marmora Terrane can be subdivided into three tectonostratigraphic units: the Schakalsberge Complex, the Oranjemund Complex and the Chameis Complex (Hartnady *et al.*, 1990). They are significantly different to the extent that they are equivalent to subterranes or may be even regarded as separate terranes within a composite Marmora super-terrane.

The Schakalsberge Complex forms the most easterly extension of the Marmora Terrane, having been thrust over the Port Nolloth zone along the SE-vergent Schakalsberge Thrust (see Fig. 2), and is composed of metabasic lavas of the Grootderm Formation, capped by dolomites of the Gais Formation. The internal stratigraphy of this complex is complicated due to intense SE-directed thrusting and sinistral shearing along a penetrative S1 foliation. Preliminary geochemical data (Smith & Hartnady, 1984; unpublished data) suggest that the Grootderm Formation originated in an oceanic intraplate environment resembling a Hawaiian-type seamount chain or a Walvis-type aseismic ridge. The lavas were intruded by the Rooilepel Bostonite Suite, predominantly in the form of dykes and sills. Growth of stromatolite reefs and deposition of the Gais Formation during the waning stages of Grootderm volcanism is evident. Metamorphism in the Schakalsberge Complex does not exceed greenschist facies.

The Oranjemund Complex is characterized by very low- to low-grade metagreywackes varying from relatively undeformed cyclothemic turbidites to intensely transposed, poly-deformed mica schists. Locally, it also includes metavolcanic chlorite schists. This complex is considered a forearc turbidite sequence.

The westernmost complex, the Chameis Complex, was reinterpreted by Hartnady *et al.* (1990) as a heterogeneous melange. Various exotic blocks from different oceanic environments are found in close proximity to each other. Ultramafic and mafic blocks, 0.1–100 m in size, occur within a highly tectonized, diverse metasedimentary envelope comprising interbedded chloritic, talcose, quartzitic, quartzo-feldspathic, dolomitic, graphitic and ferruginous schists. Some of these tectonic blocks reveal a distinct metamorphic history prior to that recorded by the metasedimentary country rocks. Ultramafics include serpentinized metapyroxenites and metaperidotites; mafic rock types include massive as well as layered metagabbros, metadolerites and metabasalts (in places amygdaloidal). Preliminary geochemical data (not shown) define a tholeiitic trend consistent with an oceanic origin.

Age relationships between the various tectonostratigraphic units of the Gariep belt are not well constrained. Intrusion of the pre-tectonic Gannakouriep dykes into the lower Gariep sediments sets a maximum age for the sedimentary sequence of *c.* 720 Ma (Reid *et al.*, 1992). K–Ar isochron ages of metamorphic amphiboles in the Gannakouriep dyke swarm and $^{40}Ar/^{39}Ar$ whole-rock ages suggest growth of these amphiboles at *c.* 540 Ma (Onstott *et al.*, 1986; Reid *et al.*, 1992). A Rb/Sr age of 492 ± 18 Ma (recalculated) has been obtained for the Rooi

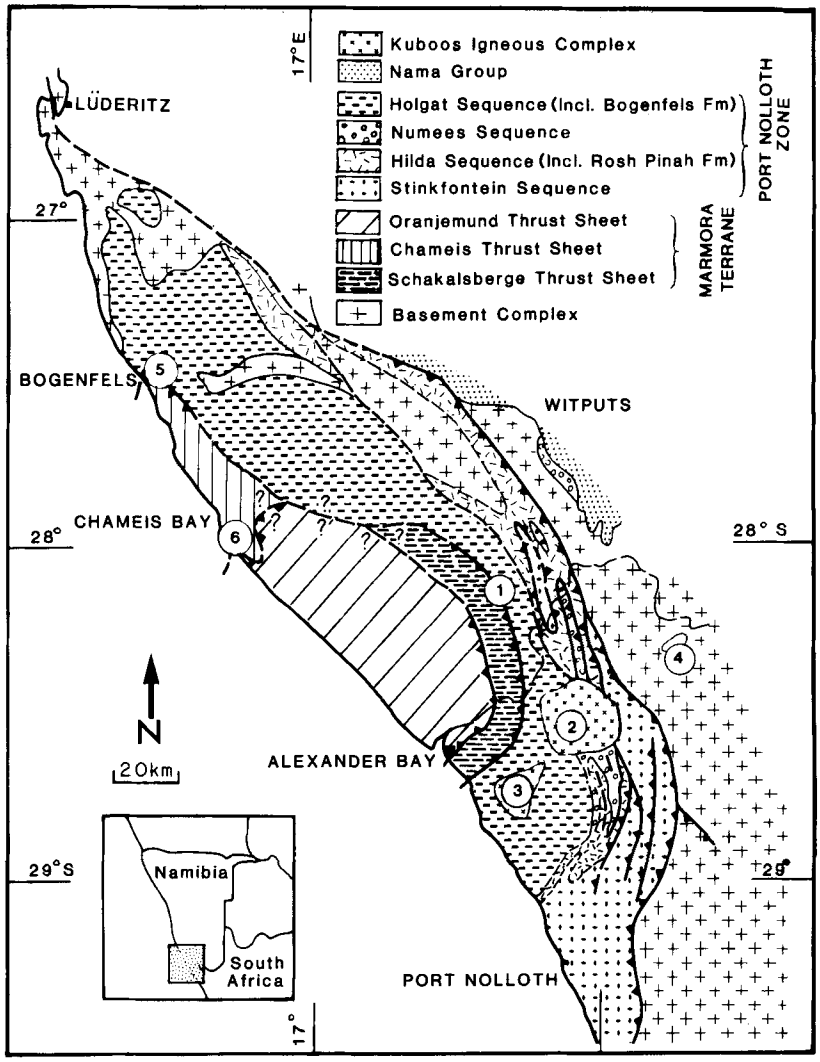

Fig. 2. Simplified geological map of the Gariep belt: 1 = Schakalsberge thrust; 2–4 = post-orogenic alkaline intrusions—Kuboos (2), Swartbank (3), Bremen (4); 5 = sample locality of 'blueschist' CHB07 at Bogenfels; 6 = sample locality of metabasalt and metagabbro IR2-5 at Chameis Bay.

Lepel bostonite (Kröner & Hawkesworth, 1976). Kröner & Welin (1973) reported a Rb/Sr age of 485 ± 15 Ma for the Bogenfels metapelites. These data are believed to represent post-tectonic regional metamorphic cooling ages rather than the age of thrusting and nappe emplacement. The clearly post-orogenic alkaline plutons along the Bremen–Kuboos line (Fig. 2) were intruded into already folded metasediments of the Port Nolloth zone and have a Rb/Sr age of 530 ± 12 Ma and a U/Pb age of 520 ± 12 Ma (Allsopp *et al.*, 1979). This sets a minimum age limit for major tectonism in the Gariep belt and hence for obduction of the Marmora Terrane onto the Port Nolloth foreland.

The Chameis Complex stretches along the coast of the Diamond Area in Namibia from Bogenfels in the north to Chameis Bay in the south (see Fig. 2) and thus includes all those localities from where glaucophanitic amphiboles were described by Kaiser (1926) and Kröner (1974). Kaiser (1926), whose lithological description of the rocks in the Diamond Area is still the most comprehensive to date, mentioned the following occurrences of blue amphiboles.

(1) Veins and dykelets of fibrous amphibole with optical properties 'close to glaucophane or crocidolite' in epidote–amphibolite from the 'Scheppkopf mountain'.

(2) Hornblende–clinochlorefels from 5 km east of the 'Onyx pan on farm Marmora' contains 'glaucophanitic hornblende', clinochlore, andesine, brown-green biotite, epidote/clinozoisite, titanite and ilmenite.

(3) Amphibolite (metabasalt) from the hills west of 'Gangkopffeld 2' contains, apart from plagioclase, epidote/clinozoisite, titanite and ilmenite, zoned amphiboles with brown cores and blue-green rims. The cores are described as 'normal hornblende' and the rims as 'glaucophanitic hornblende'.

(4) Riebeckite is described from an 'alkaliamphibolite' from the road between Buntfeldschuh and Bogenfels.

Kröner (1974) mentioned 'the occurrence of glaucophane and other Na-amphiboles in Grootderm rocks of the Bogenfels area.'

The rocks containing the blue amphiboles described here were collected from two different areas. (i) At

Weißrand, east of Bogenfels (locality 5 on Fig. 2), near the base of the Chameis thrust sheet, an exotic block approximately 2 × 1 × 0.5 m in size was found to consist of a highly schistose, dark green metabasaltic rock which grades into a rather massive, dark grey to blue rock with abundant deep blue amphiboles ('blueschist', sample CHB07). Kröner's (1974) 'glaucophane' is described from the same general locality. We therefore assume that the 'glaucophane' mentioned by him and the blue amphiboles in our sample are of similar nature. The optical properties and paragenesis of associated blue-green amphiboles in the metabasalt are in accordance with those described by Kaiser (1926) as type (3).

(ii) Amphiboles similar to the latter with a zonation from brown to blue-green were found in metagabbros at Chameis Bay (locality 6 in Fig. 2; samples IR2, 3 & 5). Metagabbro blocks at this locality occur together with a series of other tectonic blocks such as pyroxenites and peridotites (which are now largely serpentinized), and hydrothermally altered metabasalts (sample IR4).

MINERALOGY

The mineral analyses listed in Tables 1–6 were all obtained on a CAMECA electron microprobe at the Department of Geochemistry, University of Cape Town. An accelerating voltage of 15 kV and a 10-s counting time were used, and the electron beam was focused to a diameter of 1 μm for most species. A ZAF correction procedure was employed and the calculations of mineral formulae were performed using the MINFILE program of Afifi & Essene (1988). The whole-rock analysis of the 'blueschist' sample CHB07 given in Table 7 was obtained using X-ray fluorescence techniques in the Department of Geochemistry, University of Cape Town. Standards used, analytical errors and detection limits are given in Le Roex *et al.* (1981).

'Blueschist' from Bogenfels (CHB07)

An exotic block of 'blueschist', found at Weißrand near Bogenfels, consists of two different lithologies: (i) a dark blue-green, well-foliated, highly deformed metabasalt, with an assemblage of blue-green amphibole, biotite, epidote, albite, quartz, titanite, ilmenite and hematite, grading into (ii) a blue to grey, in places massive rock which consists mainly of a fine-grained, equigranular, granoblastic matrix of albite, and to a lesser extent potassic feldspar and quartz, which is overgrown by euhedral to subhedral porphyro- to poikiloblasts of dark blue to violet amphiboles, up to a few millimetres in length. Although randomly orientated in the core, the blue amphiboles are progressively aligned towards the contact with the metabasalt. Small cross-cutting veinlets of coarser albite and quartz are overgrown by the blue amphibole porphyroblasts.

Lithology I (metabasalt)

An earlier pre-tectonic assemblage consisting of amphibole I (Amph I) + plagioclase (composition?) + biotite + ilmenite + quartz was replaced syntectonically by amphibole II (Amph II) + biotite + epidote + quartz + albite + titanite + hematite.

Amphiboles occur as subhedral to anhedral porphyroclasts, up to 1 mm in diameter, and as part of the fine-grained matrix, aligned parallel to the main S1 foliation. The porphyroclasts are zoned with a brownish to pale green core (Amph I) and an intensively pleochroic rim (Amph II), with X = pale yellow, Y = dark olive green, Z = dark greenish blue. Whilst the pre-tectonic Amph I might have replaced former magmatic pyroxene, Amph II is syntectonic with a preferred lattice orientation defining a lineation L1.

Both Amph I and Amph II are calcic in composition (Table 1). Normalization assuming all iron as FeO and 24(O + OH) yields 15.2–15.9 cations with the A-site not completely filled. A slightly lower cation total is obtained by normalization based on 13 cations exclusive of K, Na

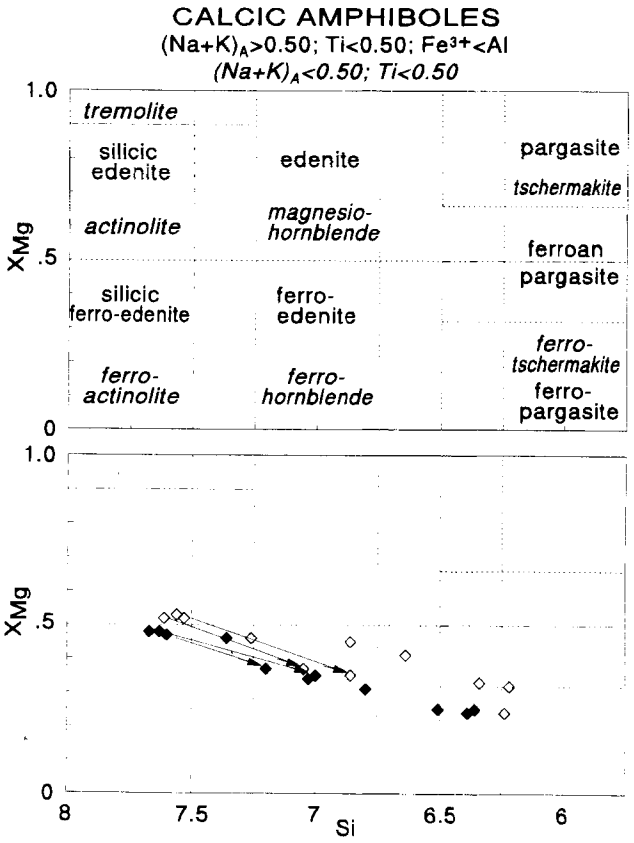

Fig. 3. Composition of amphiboles in the metabasaltic envelope of 'blueschist' (sample CHB07) from Bogenfels (see Table 1). Amphibole nomenclature after Hawthorne (1981). Arrows indicate core–rim relationships; open symbols = normalization based on 13 cations exclusive of Na, K and Ca; filled symbols = normalization based on an all-Fe^{2+} assumption and 24(O + OH).

Table 1. Electron microprobe analyses and formulae of amphiboles (generation I + II) in metabasaltic envelope of 'blueschist' from Bogenfels (sample CHB07).

	I	I	I	I	II	II	II	II	II	II	II
SiO_2	49.14	50.51	51.48	50.53	45.72	43.93	47.31	41.76	40.81	45.78	40.60
TiO_2	0.14	—	—	0.09	0.13	0.21	0.18	0.22	0.26	0.21	0.23
Al_2O_3	5.21	2.82	2.38	3.11	8.60	9.85	6.78	11.92	12.88	8.23	12.39
Cr_2O_3	—	—	—	—	—	—	—	—	—	—	—
FeO*	20.72	20.31	20.69	20.76	23.50	24.59	23.69	26.38	25.97	24.22	26.31
MnO	0.39	0.28	0.22	0.28	0.34	0.47	0.34	0.39	0.30	0.39	0.32
MgO	10.06	10.61	10.82	10.34	7.18	6.24	7.86	4.83	4.82	7.10	4.64
CaO	11.33	11.90	12.30	11.76	10.02	9.61	9.80	9.61	10.23	9.43	10.06
Na_2O	0.88	0.40	0.29	0.46	1.67	2.10	1.73	2.23	2.22	1.93	2.17
K_2O	0.28	0.14	0.10	0.17	0.45	0.54	0.27	0.88	0.93	0.45	1.02
F^-	—	—	—	—	—	—	—	—	—	—	—
Cl^-	—	—	—	—	—	—	—	—	—	—	—
Total	98.16	96.96	98.29	97.50	97.60	97.53	97.96	98.22	98.42	97.73	97.75
	a b	a b	a b	a b	a b	a b	a b	a b	a b	a b	a b
Si	7.36 7.26	7.63 7.56	7.67 7.61	7.60 7.53	7.00 6.86	6.80 6.64	7.20 7.05	6.51 6.34	6.36 6.22	7.03 6.86	6.39 6.24
Al^{IV}	0.64 0.74	0.37 0.44	0.33 0.39	0.40 0.47	1.00 1.14	1.20 1.36	0.80 0.95	1.49 1.66	1.64 1.78	0.97 1.14	1.61 1.76
T site	8.00	8.00	8.00	8.00	8.00	8.00	8.00	8.00	8.00	8.00	8.00
Al^{VI}	0.28 0.16	0.13 0.04	0.09 0.03	0.15 0.07	0.56 0.38	0.60 0.40	0.42 0.24	0.70 0.48	0.72 0.53	0.51 0.31	0.69 0.49
Fe^{3+}	— —	— 0.43	— 0.36	— 0.46	— —	— 1.08	— —	— 1.17	— 1.02	— 1.11	— —
Ti	0.02 0.02	— —	— —	0.01 —	0.01 —	0.02 0.02	0.02 0.02	0.03 0.03	0.03 0.03	0.02 0.02	0.03 0.03
Mg	2.25 2.21	2.39 2.37	2.40 2.39	2.32 2.30	1.61 1.61	1.44 1.41	1.78 1.75	1.12 1.09	1.12 1.10	1.62 1.58	1.09 1.06
Fe^{2+}	2.46 2.56	2.48 2.11	2.50 2.20	2.52 2.12	2.79 2.95	2.93 2.03	2.77 2.95	3.15 2.18	3.13 2.29	2.84 1.92	3.20 3.38
Mn	— 0.05	— 0.04	— 0.03	— 0.03	— 0.04	— 0.06	— 0.04	— 0.05	— 0.04	— 0.05	— 0.04
M1,2,3	5.00	5.00	5.00	5.00	5.00	5.00	5.00	5.00	5.00	5.00	5.00
Fe^{2+}	0.14 —	0.09 —	0.07 —	0.10 —	0.22 —	0.25 —	0.24 —	0.29 —	0.26 —	0.27 —	0.25 —
Mn	0.05 —	0.04 —	0.03 —	0.04 —	0.04 —	0.06 —	0.04 —	0.05 —	0.04 —	0.05 —	0.04 —
Ca	1.81 1.79	1.88 1.91	1.90 1.95	1.87 1.88	1.65 1.61	1.59 1.56	1.60 1.56	1.61 1.56	1.71 1.67	1.55 1.51	1.69 1.66
Na	— 0.21	— 0.09	— 0.05	— 0.12	0.09 0.39	0.09 0.44	0.11 0.44	0.06 0.44	— 0.33	0.13 0.49	— 0.34
M4 site	2.00	2.00	2.00	2.00	2.00	2.00	2.00	2.00	2.00	2.00	2.00
Ca	0.01 —	0.05 —	0.07 —	0.03 —	— —	— —	— —	— —	— —	— —	— —
Na	0.25 0.04	0.12 0.02	0.08 0.03	0.13 0.01	0.41 0.10	0.54 0.17	0.39 0.06	0.62 0.22	0.67 0.33	0.45 0.07	0.66 0.30
K	0.05 0.05	0.03 0.03	0.02 0.02	0.03 0.03	0.09 0.09	0.11 0.10	0.05 0.05	0.18 0.17	0.19 0.18	0.09 0.09	0.20 0.20
A site	0.31 0.09	0.20 0.09	0.17 0.05	0.19 0.04	0.50 0.19	0.65 0.27	0.44 0.11	0.80 0.39	0.86 0.51	0.54 0.16	0.86 0.50
X_{Mg}	0.46 0.46	0.48 0.53	0.48 0.52	0.47 0.52	0.35 0.35	0.31 0.41	0.37 0.37	0.25 0.33	0.25 0.32	0.34 0.45	0.24 0.24

* All Fe calculated as FeO.

Calculation of formulae based on: (a) an all-Fe^{2+} assumption and 24(O + OH); (b) 13 cations exclusive of K, Na and Ca.

and Ca, a procedure that has often been proposed for calcic amphiboles (e.g. Robinson *et al.*, 1982). For some of the amphiboles, this requires a relatively high Fe^{3+} content. Normalization based on 16 cations (all sites filled) yields a higher cation total than the 'all-FeO' assumption which is chemically impossible and is therefore rejected. In Fig. 3, the calculated formulae based on an all-Fe^{2+} assumption and on 13 cations excluding K, Na and Ca, respectively, are compared with the conventional amphibole nomenclature (Hawthorne, 1981). The core compositions (Amph I) are indicative of silicic (ferro-) edenite, regardless of which normalization method is used. Rim compositions (Amph II) have relatively lower Si and lower X_{Mg} values, and plot in the ferro-edenite to ferro-pargasite or hastingsite field, respectively. Amph II is more aluminous than Amph I which is inversely correlated to SiO_2 (Fig. 4a,c). Amph II is also lower in CaO compared to Amph I and correspondingly higher in $Na_2O + K_2O$ (Fig. 4b). Furthermore, Amph II is characterized by a higher crossite content than Amph I (Fig. 4d).

Fine-grained, syntectonic, olive green *biotite* is in textural equilibrium with Amph II. Metamorphic layering on a millimetre scale with biotite- and amphibole-rich layers is evident. Normalization of the chemical analyses (Table 2) based on an all-Fe^{2+} assumption leaves the octahedral sites incompletely filled (5.8–5.9 cations). Crystal-chemical limits therefore do not require any Fe for balancing the charge. Calculating all iron as Fe^{2+} gives X_{Mg} values consistently around 0.41.

Epidote as very pale yellow, fine-grained, anhedral crystals is a major constituent and is evenly distributed throughout the rock. It is relatively homogeneous and close to ideal epidote composition with $X_{Fe^{3+}}$ varying between 0.23 and 0.27 (Table 3). Pre-tectonic *ilmenite* is largely altered to leucoxene (mainly *titanite*).

Table 2. Electron microprobe analyses of biotites in metabasalts from Bogenfels (CHB07) and Chameis Bay (IR3).

	CHB07	CHB07	IR3
SiO_2	35.15	36.04	37.34
TiO_2	2.56	2.02	1.04
Al_2O_3	15.21	15.41	15.26
FeO	23.23	23.73	17.12
MnO	0.16	0.15	0.20
MgO	8.96	9.20	14.47
CaO	0.75	0.12	0.14
Na_2O	0.00	0.00	0.41
K_2O	9.15	9.31	8.83
Total	95.16	95.98	94.82
Si	5.50	5.58	5.65
Al^{IV}	2.50	2.42	2.35
T site	8.00	8.00	8.00
Al^{VI}	0.30	0.39	0.37
Ti	0.30	0.23	0.12
Fe^{2+}	3.04	3.07	3.26
Mn	0.02	0.02	0.03
Mg	2.09	2.12	2.17
O site	5.76	5.84	5.94
Ca	0.13	0.02	0.02
Na	0.00	0.00	0.12
K	1.83	1.84	1.70
A site	1.95	1.86	1.85
X_{Mg}	0.41	0.41	0.60

Formulae calculated on the basis of 24(O + OH).

Table 3. Electron microprobe analyses of epidote in metabasalts from Bogenfels (CHB07) and Chameis Bay (IR5).

	CHB07	CHB07	CHB07	IR5	IR5
SiO_2	37.84	37.97	37.90	37.60	38.35
TiO_2	—	0.13	—	0.09	0.09
Al_2O_3	24.13	24.96	22.48	27.82	28.29
Fe_2O_3	13.61	11.51	13.24	7.68	8.06
FeO	—	0.54	—	0.52	—
MnO	—	0.16	—	—	0.01
CaO	24.16	23.14	22.38	22.66	23.38
Na_2O	—	—	0.25	0.09	0.16
Total	99.74	98.41	96.85	96.46	98.50
Si	2.96	2.99	3.05	2.97	2.97
Al^{IV}	0.04	0.01	—	0.03	0.03
Z site	3.00	3.00	3.05	3.00	3.00
Al^{VI}	2.18	2.61	2.13	2.57	2.55
Fe^{3+}	0.80	0.68	0.80	0.46	0.47
Ti	—	0.01	—	0.01	0.01
Fe^{2+}	—	0.02	0.04	0.02	—
Mn	—	0.01	—	—	—
Y site	2.98	3.02	2.98	3.05	3.03
Fe^{2+}	—	0.02	—	0.02	—
Ca	2.02	1.95	1.93	1.92	1.94
Na	—	—	0.04	0.01	0.02
X site	2.02	1.98	1.97	1.95	1.97
$X_{Fe^{3+}}$	0.27	0.23	0.27	0.15	0.16

Formulae calculated for eight tetrahedral and octahedral cations.

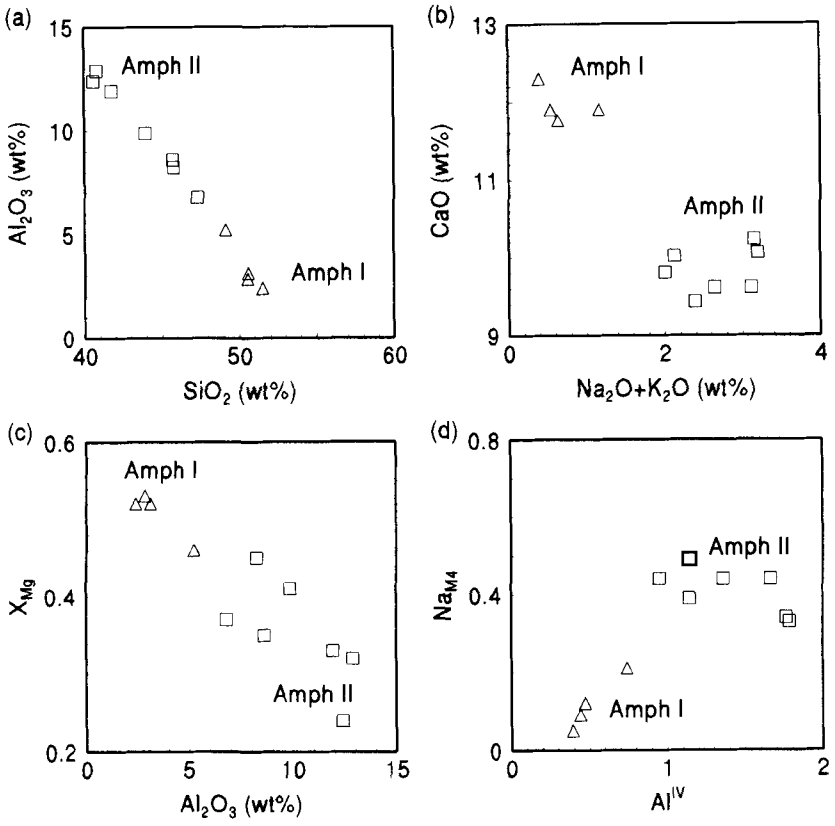

Fig. 4. Variation diagrams for composition of amphiboles in metabasalt sample CHB07 from Bogenfels. Amph I = core of phenocrysts, Amph II = rim of phenocrysts and matrix grains. In (d) the formula is normalized for Σ13 cations exclusive of K, Na and Ca, except actinolites which were normalized for 24(O + OH) and Fe_{tot} = FeO.

Lithology II ('blueschist')

Porphyro- and poikiloblasts of dark *blue amphibole*, up to 4 mm in length, are optically negative, strongly pleochroic with X = dark blue, Y = purple to yellow, Z = violet, $2V_x = 50–60°$; these parameters suggest magnesio-riebeckite. This is confirmed by the chemical analyses given in Table 4.

An all-Fe^{2+} formula calculation for 24(O + OH) yields an Si value >8.0. Fe_2O_3 was added iteratively until Si = 8.00, thus giving a minimum value for Fe^{3+}. In this case, the average $Fe^{3+}/(Fe^{3+} + Al^{VI})$ ratio of 14 crystals is 0.90 ± 0.02 and $Mg/(Mg + Fe^{2+}) = 0.63 \pm 0.02$. Calculation of Si + Al to 8.00 can give a reasonable maximum value for Fe^{3+}, assuming no Fe^{3+} in the tetrahedral position. The respective average $Fe^{3+}/(Fe^{3+} + Al^{VI})$ ratio is 0.97 ± 0.05 and $Mg/(Mg + Fe^{2+}) = 0.74 \pm 0.03$. A normalization with total cations to 15 excluding K has been considered to be effective for sodic amphiboles by Robinson *et al.* (1982). This assumption excludes Na from the A-site and forces it into M4. For the amphiboles studied here, this seems to cause an overestimation of Fe^{3+}, because it requires some Fe^{3+} to occupy tetrahedral sites while the M1–3 sites cannot be filled completely. The resulting $Fe^{3+}/(Fe^{3+} + Al^{VI})$ ratio of 1.0 and $Mg/(Mg + Fe^{2+})$ ratio of 0.86 ± 0.04 are therefore considered unlikely. Results obtained by the first method are preferred, but regardless of which method of calculating the amphibole formula is employed, all suggest magnesio-riebeckite (Fig. 5).

The fine-grained equigranular matrix consists mainly of *albite*, with 99.3–99.5 mol% Ab, 0.3–0.5% Or and 0.0–0.3% An. Quartz and traces of potassic feldspar constitute approximately 30% of the very fine-grained matrix.

Magnetite occurs throughout the rock, evenly distributed in the matrix as euhedral octahedra and rarely as inclusions within the amphibole porphyroblasts where it is rounded in form. It therefore seems that magnetite was consumed locally by the formation of the alkali amphiboles. Chemically it is a nearly ideal magnetite with no Ti, Cr, Al and Mg. However, inclusions within amphibole poikiloblasts can be slightly enriched in Ti. Many of the magnetites are oxidized to euhedral hematite, particularly along the albite–quartz veins. Pseudomorphs after an apparently short, prismatic, rhombic mineral, up to 1 mm in size, are unevenly distributed through the rock. They are dark brown (Fe-hydroxides) and consist mainly of *calcite* ($X_{Mg} = 0.09$) and *Mg-rich chlorite* of talc–chlorite composition (Table 5). In places they enclose euhedral magnetite.

An unidentified brown mineral occurs as a minor accessory phase in the form of small prismatic crystals in the matrix and inclusions within the amphiboles. It is a hydrous Fe–Mg-aluminosilicate with 3 wt% TiO_2 and 3 wt% Na_2O. It is pleochroic light to dark brown, with

Table 4. Average composition of 14 blue sodic amphibole grains in sample CHB07, 'blueschist' from Bogenfels.

	A	B	±2σ
SiO_2	54.83	54.83	0.13
TiO_2	0.06	0.06	0.06
Al_2O_3	0.77	0.77	0.02
Cr_2O_3	—	—	—
Fe_2O_3	11.00	16.49	0.35
FeO	11.95	6.97	0.32
MnO	—	—	—
MgO	11.34	11.34	0.92
ZnO	—	—	—
CaO	0.16	0.16	0.02
Na_2O	7.27	7.27	0.04
K_2O	0.21	0.21	0.01
Total	97.48	98.10	0.18
Si	7.99	7.89	
Al^{IV}	0.01	0.11	
T site	8.00	8.00	
Al^{VI}	0.12	0.03	
Fe^{3+}	1.21	1.79	
Ti	0.01	0.01	
Mg	2.46	2.43	
Fe^{2+}	1.20	0.75	
M1,2,3	5.00	5.00	
Fe^{2+}	0.26	0.09	
Ca	0.02	0.02	
Na	1.72	1.88	
M4 site	2.00	2.00	
Na	0.34	0.15	
K	0.04	0.04	
A site	0.38	0.18	
$X_{Fe^{3+}}$	0.90	0.99	
X_{Mg}	0.63	0.74	

A = minimum Fe_2O_3, B = maximum Fe_2O_3, based on normalization to Si = 8.0 and (Si + Al) = 8.0, respectively; formulae calculated for 24(O + OH).

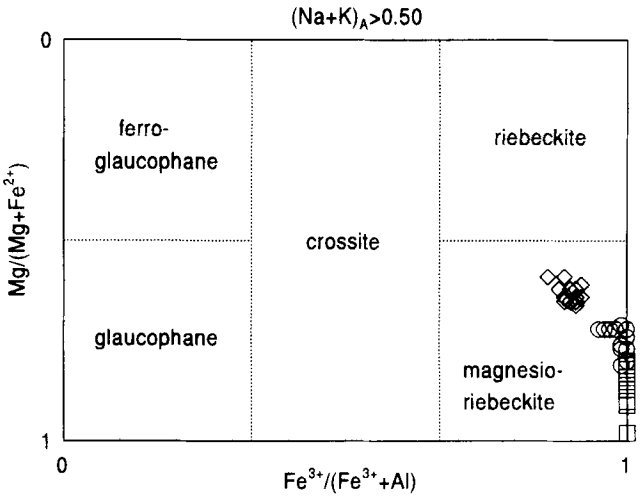

Fig. 5. Composition of blue sodic amphiboles in 'blueschist' sample CHB07 from Bogenfels (see Table 4): diamonds = normalized for a minimum Fe_2O_3 value based on crystal-chemical limits (total Si = 8.0), circles = normalized for a maximum value of Fe_2O_3 (Si + Al = 8), squares = normalization based on 15 cations exclusive of K.

	CHB07	CHB07	CHB07	CHB07	IR2	IR2	IR2	IR4	IR5
SiO_2	36.28	36.74	38.68	38.45	27.38	29.68	27.23	24.65	27.55
TiO_2	—	—	—	—	—	—	—	—	—
Al_2O_3	13.19	13.22	12.99	12.92	20.35	20.89	20.42	20.53	21.12
Cr_2O_3	—	—	—	—	1.43	—	—	—	—
FeO	10.42	8.43	10.35	10.46	15.14	15.14	15.09	30.61	15.90
MnO	—	—	—	—	0.19	0.25	0.20	0.22	0.19
MgO	24.83	25.38	23.35	23.41	23.41	24.11	23.99	12.88	22.08
CaO	0.47	0.59	0.86	0.67	—	—	—	0.22	0.07
Na_2O	0.94	1.76	0.31	0.20	0.07	—	0.08	0.14	0.14
K_2O	0.28	0.87	0.26	0.22	0.09	—	—	—	0.09
Total	86.40	87.01	86.81	86.33	86.63	90.07	87.01	89.25	87.14
Si	3.50	3.51	3.73	3.71	2.77	2.86	2.74	2.64	2.77
Al^{IV}	0.50	0.49	0.27	0.29	1.23	1.14	1.26	1.36	1.23
T site	4.00	4.00	4.00	4.00	4.00	4.00	4.00	4.00	4.00
Al^{VI}	1.04	1.04	1.21	1.18	1.19	1.24	1.16	1.22	1.28
Fe^{2+}	0.86	0.69	0.83	0.86	1.28	1.22	1.27	2.74	1.34
Mn	—	—	—	—	0.02	0.02	0.02	0.02	0.02
Mg	3.67	3.71	3.36	3.41	3.53	3.47	3.60	2.05	3.31
Ca	0.05	0.06	0.09	0.07	—	—	—	0.03	0.01
Na	0.18	0.34	0.06	0.04	0.01	—	0.02	0.03	0.03
K	0.04	0.11	0.03	0.03	0.01	—	—	—	0.01
O site	5.84	5.95	5.58	5.59	6.04	5.95	6.06	6.09	5.99

All Fe calculated as FeO; formulae normalized to 18(O + OH).

Table 5. Electron microprobe data of chlorites from metabasalt (IR4, IR5), metagabbro (IR2) and 'blueschist' (CHB07) samples.

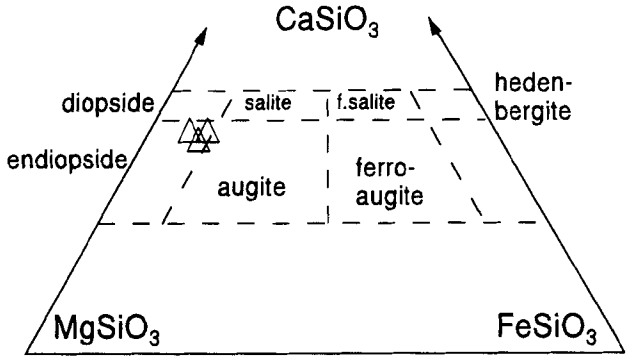

Fig. 6. Composition of clinopyroxene relics in metagabbro from Chameis Bay (triangles).

straight extinction. It appears to be highly altered, and no identification could be derived from EMP data.

The inferred equilibrium mineral assemblage for this rock is: magnesio-riebeckite + albite + quartz + calcite + chlorite + hematite.

Metabasalts and metagabbros from Chameis Bay (IR2-5)

The pre-metamorphic igneous mineral assemblage essentially consisted of plagioclase, clinopyroxene and ilmenite, with clinopyroxene relics reaching up to 3 mm in size in metagabbros. Recrystallization during multi-stage metamorphic overprint has largely destroyed the igneous textures.

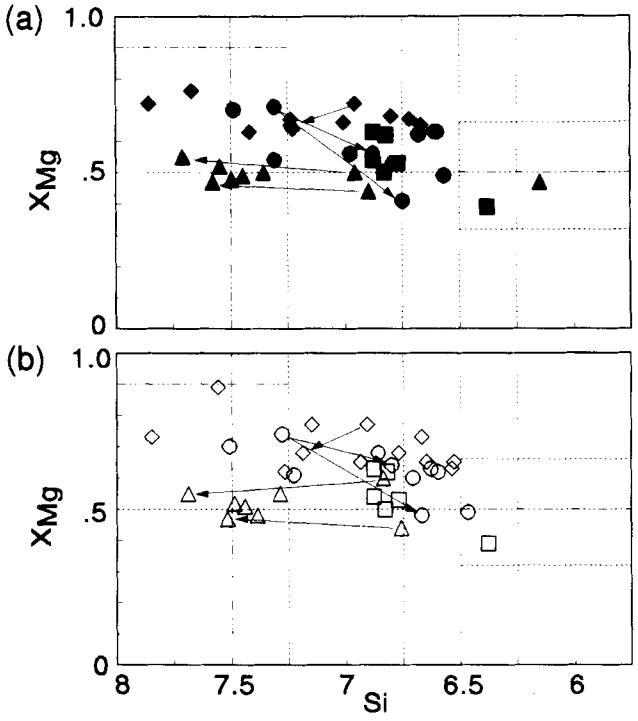

Fig. 7. Composition of amphiboles in metabasalt and metagabbro samples from Chameis Bay. For amphibole nomenclature see Fig. 3; diamonds = sample IR2, circles = sample IR3, triangles = sample IR4, squares = sample IR5—(a) normalization based on an all-Fe^{2+} assumption and 24(O + OH); (b) normalization based on 13 cations exclusive of Na, K and Ca. Arrows indicate core–rim relationships.

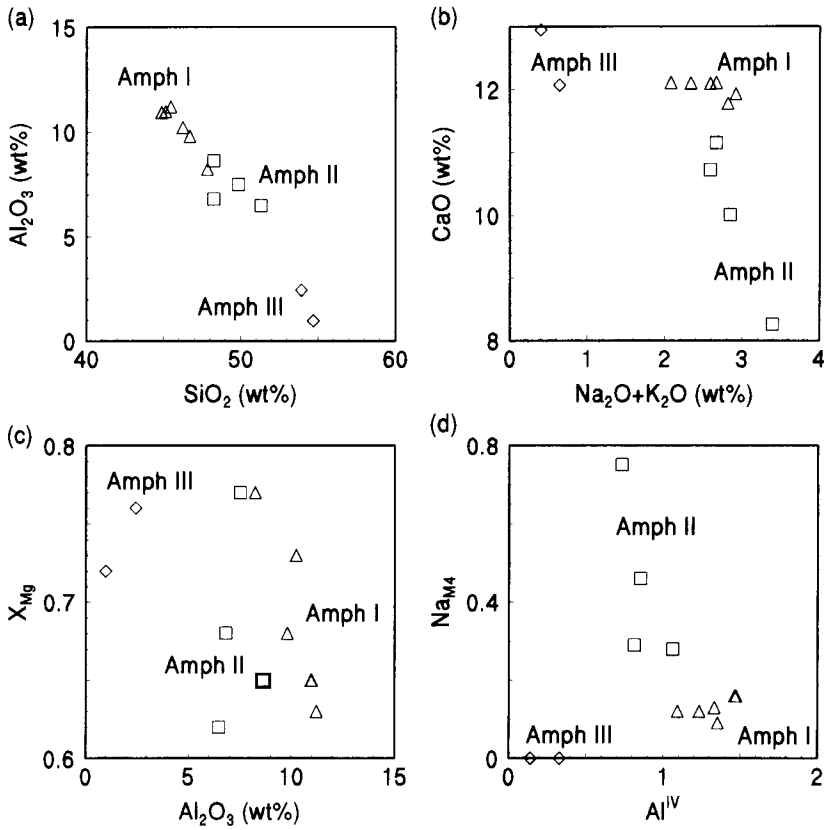

Fig. 8. Variation diagrams for composition of amphiboles in metagabbro sample IR2 from Chameis Bay; for legend see Fig. 4.

Most of the magmatic *clinopyroxene* occurs as relics in which small inclusions of titanite, aligned along its crystal faces, show a primarily euhedral habit and zonation of the former pyroxene phenocrysts. The alteration product is edenitic amphibole (see below), actinolite and/or chlorite. Relics of clinopyroxene have a pale yellow colour and are of endiopsidic composition (Fig. 6). They are slightly enriched in Al and Cr (1.6 wt% Al_2O_3 and 0.6 wt% Cr_2O_3), which is typical of magmatic clinopyroxenes. A CaO content of 21 wt% is in accordance with other cumulate clinopyroxenes from ophiolites (Hekinian, 1982).

Some traces of *biotite* occur mainly as inclusions in relic clinopyroxene or metamorphic amphibole. It often contains small rutile inclusions with sagenitic texture, indicating an initially high Ti content in the biotite. Biotite could therefore be a primary late magmatic phase or it could be of high-T hydrothermal origin. Calculating all iron as Fe^{2+} gives X_{Mg} values of *c.* 0.60 (Table 2).

Pleochroic green-blue *amphiboles* are the major constituent of the rock. They replace the clinopyroxene as pseudomorphs or form euhedral prismatic grains in the matrix. Their composition (Table 6) ranges between silicic edenite and pargasitic hornblende (Fig. 7). The formulae were calculated for both an 'all-FeO' assumption, based on 24(O + OH), and assuming 13 cations excluding K, Na and Ca.

On textural grounds, a distinction can be made between two, and in metagabbro samples, three generations of amphibole (Amph I, II, III). This is also reflected in the chemical variation between amphiboles in one and the same sample. However, each of the exotic mafic blocks studied exhibits slightly different variation in amphibole composition.

In the metagabbro samples IR2, IR3 and IR5, Amph I (cores of phenocrysts) and Amph II (rims of phenocrysts and matrix grains) show a certain variation in Al_2O_3, which is inversely correlated to SiO_2, whereby the data fields of each generation overlap each other in Figs 8(a)–10(a). On closer inspection it can be seen that in sample IR2 (Fig. 8a) Amph II is less aluminous whilst in the other two samples, IR3 and IR5 (Figs 9a & 10a), Amph II is on average slightly more aluminous with X_{Mg} being inversely correlated to Al_2O_3. The very poor correlation between X_{Mg} and Al_2O_3 in Fig. 8(c) is probably due to a certain variation in the Fe^{2+}/Fe^{3+} ratio leading to erroneous X_{Mg} values. The most obvious compositional difference between Amph I and II is a significant increase in the glaucophane [$Na_{M4} + (Al^{VI}, Fe^{3+}) = Ca + FM$] component from generation I to II (Figs 8–10b, d) leading to a more barroisitic composition.

A third amphibole generation occurs as small needles in the matrix and is distinguished chemically by its actinolitic composition (see Table 6a & Fig. 8). Amph I is characterized by the comparatively highest Ti content, Amph II has slightly lower Ti content while Amph III is almost devoid of Ti (see Table 6a).

In the one metabasalt sample studied (IR4), most of the amphiboles analysed belong to generation III. Only a few

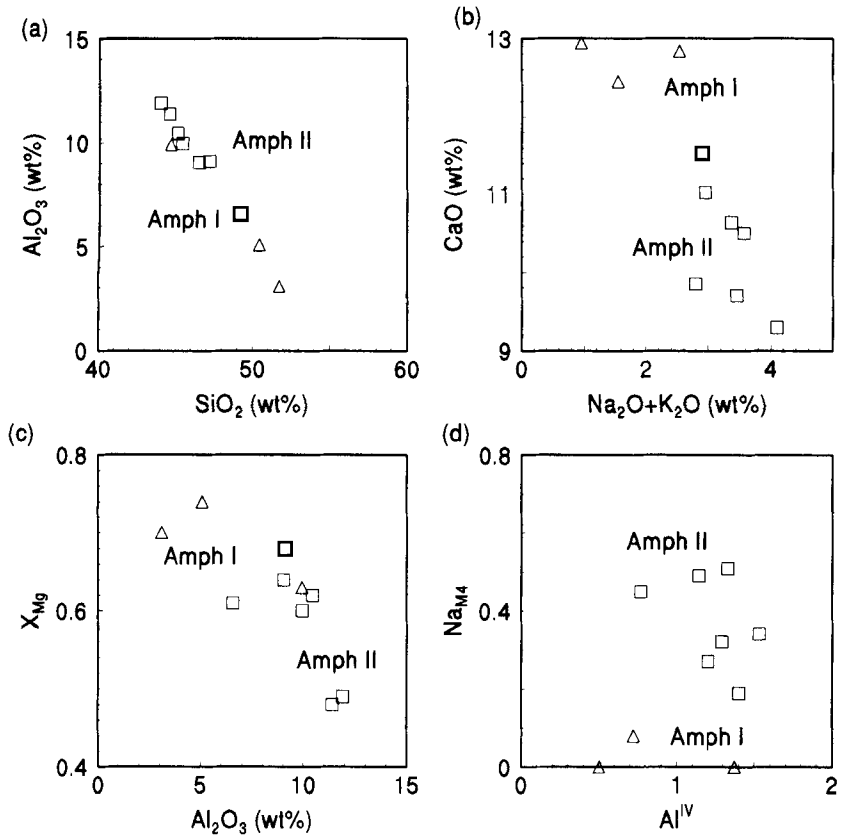

Fig. 9. Variation diagrams for composition of amphiboles in metagabbro sample IR3 from Chameis Bay; for legend see Fig. 4.

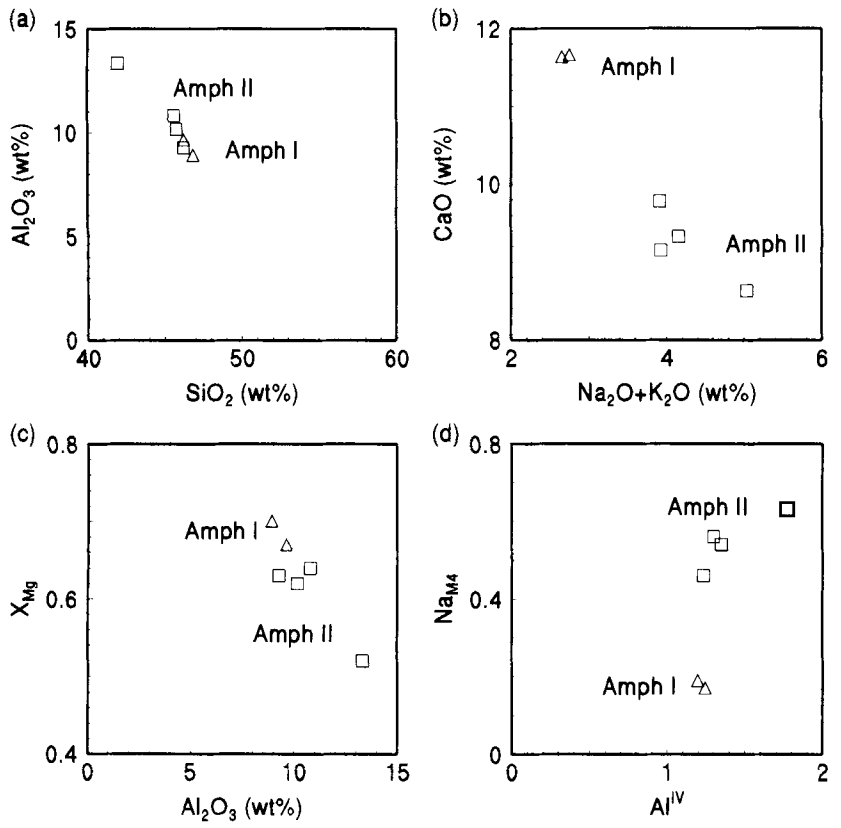

Fig. 10. Variation diagram for composition of amphiboles in metagabbro sample IR5 from Chameis Bay; for legend see Fig. 4.

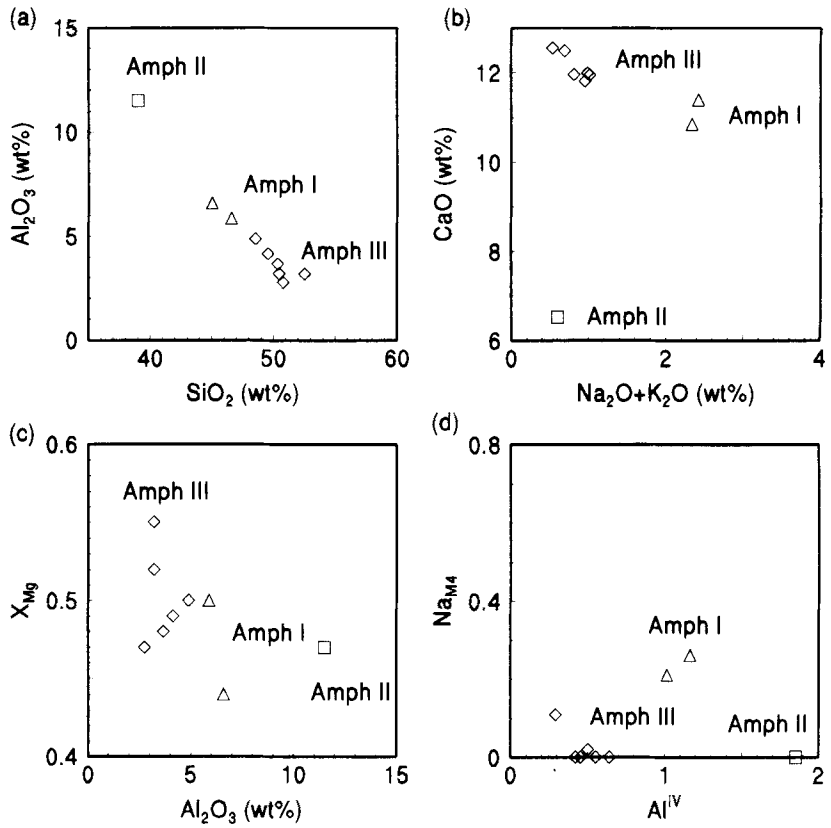

Fig. 11. Variation diagram for composition of amphiboles in metabasalt sample IR4 from Chameis Bay; for legend see Fig. 4.

representative analyses of earlier amphibole phenocrysts could be obtained. Whilst matrix amphibole and altered phenocrysts (generation III) have actinolitic compositions, relics of the earlier generation(s) are more aluminous. Amongst the latter, it appears that two distinct populations can be differentiated (Fig. 11). Bearing in mind the small number of analyses, the more calcic and more sodic but less aluminous group is tentatively classified as generation I. This amphibole (I) is also distinguished from Amph II by its much higher Ti content (see Table 6d).

Chlorite is a minor constituent of the matrix and can replace amphiboles I and II, and in some gabbro samples it pseudomorphs prismatic phenocrysts (orthopyroxene?). It has an anomalous brown interference colour and a compositional range from ripidolite to pycnochlorite (Table 5). The X_{Mg} values are between 0.71 and 0.74, and some contain a considerable amount of Cr (1.14–1.43 wt% Cr_2O_3).

All the primary plagioclase has recrystallized completely to albite ($Ab_{97-99}An_{03-01}Or_{00}$), which now forms part of the matrix. Epidote is commonly associated with the alteration of plagioclase and has $X_{Fe^{3+}}$ values around 0.15 (Table 3). Minor amounts of quartz occur together with albite in the matrix. Primary ilmenite is largely altered to leucoxene. Apart from traces of late hematite, Fe-oxides are absent.

METAMORPHIC HISTORY

Textural and compositional relations provide a basis for the distinction between different metamorphic events that have affected the mafic igneous precursor rocks of the exotic blocks (Fig. 12). The earliest recognizable metamorphic event (M1) is represented by the pre-tectonic (with regard to S1) replacement of magmatic clinopyroxene by edenitic amphiboles or hornblende. The formation of brown Ti-rich biotite may be attributed to M1 or to a previous late magmatic phase. A first alteration of magmatic plagioclase was presumably associated with M1 but cannot be distinguished from later metamorphic events.

The breakdown of clinopyroxene to calcic aluminous amphiboles indicates temperatures of 500–750 °C (Spear, 1981; Apted & Liou, 1983; Moody *et al.*, 1983). An extremely low crossite content in amphiboles I, found in all samples studied, suggests very low pressures. From the empirical geobarometer of Brown (1977), a pressure of <2 kbar is suggested for this metamorphic event (M1), assuming a fully buffered assemblage (see below).

All assemblages contain ilmenite that is altered to titanite (leucoxene). All amphibole grains can thus be considered saturated with Ti, and variations in the Ti content are probably related to metamorphic grade (Sivell & Waterhouse, 1984). Ti content is highest (up to 0.19 Ti atoms pfu) in cores of large amphiboles replacing clinopyroxene, suggesting they formed at amphibolite facies, but do not reach values usually found in magmatic hornblendes (>0.23 Ti atoms pfu; Sivell & Waterhouse, 1984). However, the Ti content varies considerably in different samples between 0 (sample IR2) and 1.67 wt% TiO_2 (sample IR3), suggesting amphibole formation in the

Table 6. Electron microprobe data of amphiboles (generation I, II and III) in metagabbro and metabasalt samples from Chameis Bay.

	(a) Metagabbro (IR2)											
	I	I	I	I	I	I	II	II	II	II	III	III
SiO_2	45.12	46.23	45.45	47.82	44.85	46.68	48.24	51.30	48.23	49.84	53.93	54.71
TiO_2	0.23	0.29	0.15	0.45	0.26	0.45	0.11	0.11	0.24	0.14	0.13	—
Al_2O_3	10.98	10.21	11.20	8.22	10.93	9.79	6.80	6.48	8.62	7.50	2.42	0.97
Cr_2O_3	0.48	0.87	—	0.53	1.24	0.73	—	—	—	—	—	—
FeO	12.48	11.96	13.76	10.69	12.78	11.48	13.19	14.63	13.21	12.49	10.27	11.63
MnO	0.21	0.18	0.22	0.20	0.18	0.20	0.21	0.20	0.25	0.21	0.17	0.13
MgO	12.72	13.98	13.31	15.14	13.14	13.93	13.23	13.61	13.72	14.26	18.22	16.72
CaO	12.11	12.09	11.93	12.11	11.78	12.10	10.72	8.26	11.15	10.01	12.07	12.95
Na_2O	2.28	2.28	2.53	1.90	2.46	2.14	2.21	3.13	2.34	2.50	0.46	0.30
K_2O	0.38	0.30	0.38	0.17	0.35	0.19	0.37	0.26	0.32	0.34	0.18	0.10
Total	96.98	98.39	98.93	97.23	97.97	97.69	95.08	97.98	98.08	97.29	97.84	97.51
	a b	a b	a b	a b	a b	a b	a b	a b	a b	a b	a b	a b
Si	6.67 6.65	6.72 6.67	6.62 6.54	6.96 6.91	6.59 6.53	6.80 6.77	7.23 7.19	7.42 7.27	7.01 6.94	7.24 7.15	7.67 7.56	7.86 7.85
Al^{IV}	1.33 1.35	1.28 1.33	1.38 1.46	1.04 1.09	1.41 1.47	1.20 1.23	0.77 0.81	0.58 0.73	0.99 1.06	0.76 0.85	0.33 0.40	0.14 0.15
T site	8.00 8.00	8.00 8.00	8.00 8.00	8.00 8.00	8.00 8.00	8.00 8.00	8.00 8.00	8.00 8.00	8.00 8.00	8.00 8.00	8.00 8.00	8.00 8.00
Al^{VI}	0.58 0.56	0.46 0.40	0.54 0.44	0.37 0.31	0.48 0.40	0.48 0.44	0.43 0.38	0.53 0.35	0.49 0.41	0.52 0.41	0.08 —	0.02 0.01
Fe^{3+}	— 0.34	— 0.30	— —	— —	— —	— —	— 0.28	— 0.63	— 0.58	— —	— —	— 0.06
Ti	0.03 0.02	0.03 0.03	0.02 0.02	0.05 0.05	0.03 0.03	0.05 0.05	0.01 0.01	0.01 0.01	0.03 0.03	0.02 0.01	0.01 0.01	— —
Cr	0.06 0.06	0.10 0.10	— —	0.06 0.06	0.14 0.08	0.08 —	— —	— —	— —	— 0.14	— —	— —
Mg	2.80 2.80	3.03 3.00	2.89 2.86	3.28 3.26	2.88 2.85	3.02 3.01	2.96 2.94	2.94 2.88	2.97 2.95	3.09 3.05	3.86 3.81	3.58 3.58
Fe^{2+}	1.53 1.54	1.38 1.10	1.55 1.66	1.24 0.99	1.47 1.56	1.36 1.39	1.60 1.36	1.53 1.73	1.51 1.59	1.38 0.92	1.05 0.53	1.40 1.34
Mn	— 0.03	— 0.02	— 0.03	— 0.02	— 0.02	— 0.02	— 0.03	— 0.02	— 0.03	— 0.03	— 0.02	— 0.02
M1,2,3	5.00 5.00	5.00 5.00	5.00 5.00	5.00 5.00	5.00 5.00	5.00 5.00	5.00 5.00	5.00 5.00	5.00 5.00	5.00 5.00	5.00 5.00	5.00 5.00
Mg	— —	— —	— —	— —	— —	— —	— —	— —	— —	— —	— —	— —
Fe^{2+}	0.01 —	0.08 —	0.12 —	0.06 —	0.10 —	0.04 —	0.05 —	0.25 —	0.10 —	0.14 —	0.17 —	— —
Mn	0.03 —	0.02 —	0.03 —	0.02 —	0.02 —	0.02 —	0.03 —	0.02 —	0.03 —	0.03 —	0.02 —	0.02 —
Ca	1.92 1.91	1.88 1.87	1.85 1.84	1.89 1.88	1.85 1.84	1.89 1.88	1.72 1.71	1.28 1.25	1.74 1.72	1.56 1.54	1.81 1.81	1.98 1.99
Na	0.04 0.09	0.02 0.13	— 0.16	0.03 0.12	0.02 0.16	0.05 0.12	0.20 0.29	0.45 0.75	0.14 0.28	0.28 0.46	— 0.12	— 0.01
M4 site	2.00 2.00	2.00 2.00	2.00 2.00	2.00 2.00	2.00 2.00	2.00 2.00	2.00 2.00	2.00 2.00	2.00 2.00	2.00 2.00	2.00 1.94	2.00 2.00
Ca	— —	— —	0.01 —	— —	— —	— —	— —	— —	— —	— —	0.03 —	0.01 —
Na	0.61 0.56	0.62 0.51	0.71 0.55	0.51 0.41	0.68 0.53	0.55 0.48	0.44 0.35	0.43 0.11	0.52 0.37	0.43 0.23	0.13 —	0.08 0.07
K	0.07 0.07	0.06 0.06	0.07 0.07	0.03 0.03	0.07 0.06	0.04 0.04	0.07 0.07	0.05 0.05	0.06 0.06	0.06 0.06	0.03 0.03	0.02 0.02
A site	0.68 0.64	0.68 0.56	0.80 0.62	0.54 0.44	0.75 0.60	0.59 0.52	0.51 0.42	0.48 0.16	0.58 0.43	0.49 0.30	0.19 0.03	0.11 0.09
X_{Mg}	0.65 0.65	0.67 0.73	0.63 0.63	0.72 0.77	0.65 0.65	0.68 0.68	0.64 0.68	0.63 0.62	0.66 0.65	0.67 0.77	0.76 0.88	0.72 0.73

Table 6. (Continued)

	(b) Metagabbro (IR3)									
	I	I	I	II	II	II	II	II	II	II
SiO_2	51.73	50.41	44.66	49.20	43.97	47.23	45.44	45.12	46.53	44.59
TiO_2	1.33	0.31	1.67	0.11	0.13	0.10	0.12	0.14	0.30	0.00
Al_2O_3	3.08	5.08	9.93	6.57	11.91	9.09	9.96	10.45	9.04	11.38
Cr_2O_3	—	0.18	0.35	—	—	—	—	—	—	—
FeO	11.96	11.53	13.08	17.21	18.42	16.29	17.12	14.15	16.42	20.24
MnO	0.20	0.18	0.17	0.27	0.25	0.29	0.24	0.28	0.22	0.20
MgO	15.46	15.75	12.51	11.25	9.80	11.80	10.87	12.92	11.83	7.95
CaO	12.94	12.44	12.83	9.85	10.50	9.70	10.64	11.54	11.02	9.29
Na_2O	0.85	1.40	2.23	2.46	3.07	3.02	3.00	2.53	2.57	3.39
K_2O	0.10	0.15	0.30	0.33	0.50	0.44	0.37	0.37	0.38	0.70
Total	97.66	97.43	97.73	97.26	98.56	97.94	97.76	97.51	98.31	97.74
	a b	a b	a b	a b	a b	a b	a b	a b	a b	a b
Si	7.49 7.51	7.31 7.28	6.60 6.63	7.31 7.23	6.57 6.47	6.98 6.86	6.79 6.71	6.68 6.60	6.88 6.80	6.75 6.67
Al^{IV}	0.51 0.49	0.69 0.72	1.40 1.37	0.69 0.77	1.43 1.53	1.02 1.14	1.21 1.29	1.32 1.40	1.12 1.20	1.25 1.33
T site	8.00 8.00	8.00 8.00	8.00 8.00	8.00 8.00	8.00 8.00	8.00 8.00	8.00 8.00	8.00 8.00	8.00 8.00	8.00 8.00
Al^{VI}	0.01 0.03	0.18 0.14	0.33 0.36	0.46 0.37	0.66 0.54	0.56 0.42	0.54 0.45	0.51 0.40	0.45 0.36	0.78 0.67
Fe^{3+}	— —	— 0.23	— —	— 0.50	— —	— 0.75	— 0.51	— —	— 0.53	— 0.57
Ti	0.14 0.15	0.03 0.03	0.19 0.19	0.01 0.01	0.01 0.01	0.01 0.01	0.01 0.01	0.02 0.02	0.03 0.03	— —
Cr	— —	0.02 0.02	0.04 0.04	— —	— —	— —	— —	— —	— —	— —
Mg	3.34 3.34	3.41 3.39	2.76 2.77	2.49 2.47	2.18 2.15	2.60 2.56	2.42 2.39	2.85 2.82	2.61 2.58	1.79 1.77
Fe^{2+}	1.45 1.45	1.36 1.17	1.62 1.62	2.03 1.61	2.14 2.27	1.83 1.23	2.02 1.60	1.63 1.73	1.91 1.48	2.43 1.96
Mn	0.02 0.02	— 0.02	0.02 0.02	— 0.03	0.00 0.03	— 0.04	— 0.03	— 0.03	— 0.03	— 0.03
Ca	0.03 0.03	0.00 —	0.05 —	0.00 —	— —	— —	— —	— —	— —	— —
M1,2,3	5.00 5.03	5.00 5.00	5.00 5.00	5.00 5.00	5.00 5.00	5.00 5.00	5.00 5.00	5.00 5.00	5.00 5.00	5.00 5.00
Fe^{2+}	— —	0.04 —	— —	0.11 —	0.16 —	0.18 —	0.12 —	0.13 —	0.12 —	0.14 —
Mn	— —	0.02 —	— —	0.03 —	0.03 —	0.04 —	0.03 —	0.03 —	0.03 —	0.03 —
Ca	2.00 2.00	1.93 1.92	2.00 2.00	1.57 1.55	1.68 1.66	1.53 1.51	1.70 1.68	1.83 1.81	1.75 1.73	1.51 1.49
Na	— —	— 0.08	— —	0.29 0.45	0.12 0.34	0.25 0.49	0.15 0.32	0.01 0.19	0.10 0.27	0.33 0.51
M4 site	2.00 2.00	2.00 2.00	2.00 2.00	2.00 2.00	2.00 2.00	2.00 2.00	2.00 2.00	2.00 2.00	2.00 2.00	2.00 2.00
Ca	— —	— —	— 0.04	— —	— —	— —	— —	— —	— —	— —
Na	0.24 0.24	0.39 0.32	0.64 0.64	0.42 0.25	0.77 0.53	0.61 0.36	0.72 0.54	0.72 0.53	0.63 0.45	0.66 0.47
K	0.02 0.02	0.03 0.03	0.06 0.06	0.06 0.06	0.10 0.09	0.08 0.08	0.07 0.07	0.07 0.07	0.07 0.07	0.13 0.13
A site	0.23 0.27	0.42 0.34	0.68 0.74	0.49 0.32	0.86 0.63	0.70 0.44	0.79 0.61	0.79 0.60	0.70 0.52	0.80 0.60
X_{Mg}	0.70 0.70	0.71 0.74	0.63 0.63	0.54 0.61	0.49 0.49	0.56 0.68	0.53 0.60	0.62 0.62	0.56 0.64	0.41 0.48

Table 6. (Continued)

(c) Metagabbro (IR5)						
	I	I	II	II	II	II
SiO_2	46.23	46.83	45.59	46.21	45.76	41.96
TiO_2	0.22	0.20	0.13	0.15	0.08	—
Al_2O_3	9.62	8.89	10.79	9.24	10.15	13.30
Cr_2O_3	—	0.14	—	—	—	—
FeO	14.19	13.99	17.04	17.28	18.59	21.52
MnO	0.20	0.22	0.36	0.20	0.30	0.36
MgO	12.81	13.35	10.80	11.30	10.24	7.76
CaO	11.65	11.63	9.33	9.78	9.15	8.63
Na_2O	2.43	2.37	3.69	3.44	3.54	4.22
K_2O	0.32	0.28	0.46	0.47	0.38	0.81
Total	97.68	97.92	98.21	98.08	98.18	98.56
	a b	a b	a b	a b	a b	a b
Si	6.82 6.76	6.88 6.81	6.77 6.65	6.88 6.77	6.83 6.70	6.38 6.23
Al^{IV}	1.18 1.24	1.12 1.19	1.23 1.35	1.12 1.23	1.17 1.30	1.62 1.77
T site	8.00 8.00	8.00 8.00	8.00 8.00	8.00 8.00	8.00 8.00	8.00 8.00
Al^{VI}	0.49 0.42	0.42 0.34	0.65 0.51	0.50 0.37	0.61 0.45	0.77 0.56
Fe^{3+}	— 0.37	— 0.44	— 0.75	— 0.68	— 0.90	— 1.09
Ti	0.02 0.02	0.02 0.02	0.01 0.01	0.02 0.02	0.01 0.01	— —
Cr	— —	0.02 0.02	— —	— —	— —	— —
Mg	2.82 2.79	2.92 2.90	2.39 2.35	2.51 2.47	2.28 2.23	1.76 1.72
Fe^{2+}	1.67 1.37	1.62 1.26	1.94 1.33	1.98 1.44	2.10 1.38	2.47 1.58
Mn	— 0.02	— 0.03	— 0.04	— 0.02	— 0.04	— 0.04
M1,2,3	5.00 5.00	5.00 5.00	5.00 5.00	5.00 5.00	5.00 5.00	5.00 5.00
Fe^{2+}	0.08 —	0.10 —	0.17 —	0.17 —	0.22 —	0.27 —
Mn	0.03 —	0.03 —	0.05 —	0.02 —	0.04 —	0.05 —
Ca	1.84 1.83	1.83 1.81	1.48 1.46	1.56 1.54	1.46 1.44	1.41 1.37
Na	0.05 0.17	0.04 0.19	0.30 0.54	0.25 0.46	0.28 0.56	0.28 0.63
M4 site	2.00 2.00	2.00 2.00	2.00 2.00	2.00 2.00	2.00 2.00	2.00 2.00
Na	0.64 0.52	0.63 0.48	0.76 0.51	0.75 0.52	0.75 0.44	0.97 0.59
K	0.06 0.06	0.05 0.05	0.09 0.09	0.09 0.09	0.07 0.07	0.16 0.15
A site	0.70 0.58	0.69 0.53	0.85 0.60	0.84 0.61	0.82 0.51	1.12 0.74
X_{Mg}	0.62 0.67	0.63 0.70	0.53 0.64	0.54 0.63	0.50 0.62	0.39 0.52

various mafic blocks during M1 over a wide range of temperatures. This is supported by the relatively wide range of Al^{IV} values calculated (0.4–1.5) which is mainly a function of temperature (Brown, 1977; Blundy & Holland, 1990). Because the actual composition of plagioclase in equilibrium with Amph I is not preserved, Blundy & Holland's (1990) geothermometer cannot be applied. If the number of Si atoms pfu is mainly a function of temperature (Blundy & Holland, 1990) and assuming that the plagioclase composition changes from albite at upper greenschist facies to oligoclase at amphibolite facies conditions, becoming progressively more calcic with increasing metamorphic grade, some constraints on the range of possible temperatures of amphibole formation can be estimated from the Si numbers calculated. Amph I in samples CHB07 and IR3 seems to have grown at temperatures of 500–650° C, whereas those in samples IR2 and IR5 were formed at higher temperatures, i.e. *c.* 700° C.

These temperatures, together with the very low pressure inferred and the fact that M1 is the first metamorphic imprint on the igneous precursor, strongly suggest that M1 represents a hydrothermal oceanic metamorphic event during which basalts and gabbros were hydrated to greenschist, epidote-amphibolite and amphibolite at various temperatures. A geothermal gradient of up to $300° C\,km^{-1}$ can be derived from the temperatures and pressures estimated above. Similarly high gradients have been described for very early hydrothermal metamorphism, immediately following crystallization of the mafic magma, in the Atlantic, Pacific and Indian Oceans and the Caribbean (Ito & Anderson, 1983; Sivell & Waterhouse, 1984; Herbert & Constantin, 1991).

The compositional change from Amph I to Amph II reflects a second metamorphic event M2 superimposed onto the M1 parageneses. The compositional trend from Amph I to Amph II is, however, different in each of the exotic blocks investigated. For instance, amphiboles from samples CHB07, IR3 and IR5 show a trend towards higher edenite ($Na_A + Al^{IV} = \square + Si$) component as opposed to those in sample IR2. In all samples except IR2, Amph II is richer in the Tschermak [$(Al^{VI}, Fe^{3+}) + Al^{IV} = Si + FM$] component.

These two trends are considered to indicate an

Table 6. (Continued)

	(d) Metabasalt (IR4)								
	I	I	II	III	III	III	III	III	III
SiO_2	45.01	46.55	39.00	50.75	49.53	48.50	52.51	50.31	50.42
TiO_2	1.44	1.44	0.15	0.00	0.12	0.12	0.00	0.00	0.18
Al_2O_3	6.58	5.86	11.50	2.75	4.14	4.87	3.19	3.66	3.18
Cr_2O_3	0.00	0.00	0.89	0.00	0.19	0.00	0.00	0.00	0.29
FeO	21.62	20.13	24.50	21.42	19.86	19.00	17.50	20.73	18.89
MnO	0.30	0.25	0.22	0.17	0.25	0.25	0.20	0.23	0.30
MgO	9.63	11.31	12.16	10.55	10.48	10.78	11.90	10.56	11.35
CaO	10.84	11.38	6.51	12.54	11.98	11.94	11.80	12.48	11.95
Na_2O	1.54	1.46	0.44	0.38	0.76	0.81	0.82	0.47	0.66
K_2O	0.79	0.95	0.16	0.15	0.22	0.20	0.13	0.22	0.15
Total	97.74	99.33	95.52	98.71	97.55	96.46	98.05	98.66	97.37
	a b	a b	a*	a b	a b	a b	a b	a b	a b	a b
Si	6.90 6.76	6.96 6.84	6.15	7.58 7.52	7.45 7.39	7.36 7.29	7.71 7.69	7.50 7.44	7.55 7.49
Al^{IV}	1.10 1.16	1.03 1.01	1.85	0.42 0.48	0.55 0.61	0.64 0.71	0.29 0.31	0.50 0.56	0.45 0.51
Fe^{3+}	— —	— 0.14	—	— —	— —	— —	— —	— —	— —
Ti	— 0.07	— —	—	— —	— —	— —	— —	— —	— —
T site	8.00 8.00	8.00 8.00	8.00	8.00 8.00	8.00 8.00	8.00 8.00	8.00 8.00	8.00 8.00	8.00 8.00
Al^{VI}	0.08 —	— —	0.28	0.06 —	0.18 0.12	0.23 0.15	0.26 0.24	0.14 0.08	0.11 0.05
Fe^{3+}	— —	— 0.66	—	— —	— —	— 0.42	— —	— 0.35	— —
Ti	0.07 0.09	0.16 0.16	0.02	— —	0.01 0.01	0.01 0.01	— —	— —	0.02 0.02
Cr	— —	— —	0.11	— —	0.02 0.02	— —	— —	— —	0.03 0.03
Mg	2.20 2.16	2.52 2.48	2.86	2.35 2.33	2.35 2.33	2.44 2.42	2.60 2.60	2.35 2.33	2.53 2.51
Fe^{2+}	2.55 2.72	2.32 1.67	1.73	2.59 2.65	2.43 2.48	2.32 1.97	2.14 2.14	2.51 2.21	2.30 2.35
Mn	— 0.04	— 0.03	—	— 0.02	— 0.03	— 0.03	— 0.02	— 0.03	— 0.04
M1,2,3	5.00 5.00	5.00 5.00	5.00	5.00 5.00	5.00 5.00	5.00 5.00	5.00 5.00	5.00 5.00	5.00 5.00
Fe^{2+}	0.22 —	0.20 —	1.50	0.08 —	0.07 —	0.09 —	0.01 —	0.07 —	0.07 —
Mn	0.04 —	0.03 —	0.03	0.02 —	0.03 —	0.03 —	0.02 —	0.03 —	0.04 —
Ca	1.74 1.74	1.77 1.79	0.47	1.89 1.99	1.90 1.92	1.88 1.92	1.86 1.85	1.90 1.98	1.90 1.90
Na	— 0.26	— 0.21	—	— 0.01	— 0.08	— 0.08	0.11 0.15	0.00 0.02	— 0.10
M4 site	2.00 2.00	2.00 2.00	2.00	2.00 2.00	2.00 2.00	2.00 2.00	2.00 2.00	2.00 2.00	2.00 2.00
Ca	0.04 —	0.06 —	0.63	0.11 —	0.03 —	0.06 —	— —	0.09 —	0.02 —
Na	0.46 0.19	0.42 0.21	0.13	0.11 0.10	0.22 0.14	0.24 0.16	0.12 0.08	0.13 0.11	0.19 0.09
K	0.15 0.15	0.18 0.18	0.03	0.03 0.03	0.04 0.04	0.04 0.04	0.02 0.02	0.04 0.04	0.03 0.03
A site	0.65 0.34	0.66 0.39	0.79	0.25 0.13	0.29 0.18	0.34 0.20	0.14 0.10	0.26 0.15	0.24 0.12
X_{Mg}	0.44 0.44	0.50 0.60	0.47	0.47 0.47	0.49 0.48	0.50 0.55	0.55 0.55	0.48 0.51	0.52 0.52

All Fe expressed as FeO; normalization based on (a) an all-Fe^{2+} assumption and 24(O + OH + F + Cl) and (b) on 13 cations exclusive of K, Na and Ca.
* Normalization based on Σ13 cations exclusive of K, Na and Ca gives a formula that is beyond crystal-chemical limits and is therefore rejected.

increase in metamorphic grade (Spear, 1981; Apted & Liou, 1983; Moody *et al.*, 1983). This appears to contradict the observed trend in Ti which, on average, decreases from Amph I to Amph I.

The explanation may lie in the most striking difference between the two generations, i.e. an apparent trend towards a higher glaucophane [$Na_{M4} + (Al^{VI}, Fe^{3+}) = Ca +$ FM] component observed in all samples (see Figs 4d & 8–10d). This trend suggests a significant increase in pressure from M1 to between 4 and 6 kbar for M2 (Brown, 1977; Laird, 1980; Apted & Liou, 1983). Application of the empirical geobarometer of Brown (1977) is restricted by the fact that not all assemblages contain chlorite and Fe-oxide with the latter phase usually absent. The fully buffered amphibole coexists with epidote, albite, chlorite and Fe-oxide. According to Brown (1977), the crossite component in Ca-amphibole is reduced if this reaction assemblage lacks Fe-oxide. Pressures estimated from the Na_{M4} number are therefore minima. Burial to about 15–20 km, as recorded by the increase in crossite content, was accompanied in some blocks (CHB07, IR3 & IR5) by an increase in temperature, in others (IR2) by a decrease in temperature, depending on the temperature achieved during M1 in the particular block. This is reflected in the variation in Ti which not only appears to be mainly a function of temperature and f_{O_2} (Spear, 1981), but was found to be concentrated in calcic amphibole compared to coexisting sodic amphibole by Ernst (1979). Alteration of ilmenite to leucoxene is widespread and common in all samples. This requires a decrease in temperature and/or increase in f_{O_2} and f_{H_2O}. According to the experimental results of Spear (1981), amphibole + ilmenite + titanite are stable together at temperatures of <580° C. Application of Blundy & Holland's (1990) amphibole–plagioclase geothermometer to the syntectonic calcic Amph II generation yields temperatures of 500–600° C for a pressure range of

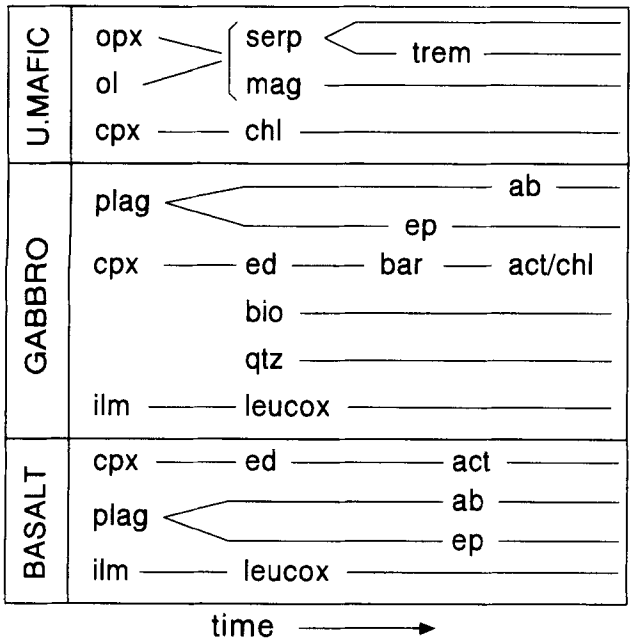

Fig. 12. Mineral assemblages and sequence of alteration in ultramafic, gabbro and basalt blocks (ab = albite, act = actinolite, bar = barroisitic hornblende, bio = biotite, chl = chlorite, cpx = clinopyroxene, ed = edenitic hornblende, ep = epidote, ilm = ilmenite, leucox = leucoxene, mag = magnetite, ol = olivine, opx = orthopyroxene, qtz = quartz, serp = serpentine, trem = tremolite).

4–6 kbar. The albitic composition of plagioclase observed agrees with the lower temperature limit. A change from a more calcic plagioclase during M2 to albite only during subsequent low-grade M3 metamorphism cannot be ruled out, therefore allowing for amphibolite facies temperatures during M2. Considering that M2 is recorded only in the exotic blocks but not in their sedimentary envelope, these results are, despite the large error involved in the P–T estimates, strong evidence for M2 being a response to a process of shallow subduction subsequent to earlier sea-floor metamorphism (M1).

The metabasalt sample IR4 differs in its metamorphic history from the metagabbros in so far that it does not reflect the M2 event. It exhibits an Amph II generation which follows a completely different trend compared to those in the metagabbro samples. It is much poorer in both CaO and ($Na_2O + K_2O$), in contrast to trends normally observed with a change in metamorphic grade (Spear, 1981; Moody *et al.*, 1983; Apted & Liou, 1983). Amph II is believed to be a product of metasomatism on the ocean floor immediately following the M1 event and not related to M2.

The latest formation of pure actinolite (Amph II) and/or chlorite at the expense of aluminous amphibole (generations I and II) can be attributed to regional low-grade (lower greenschist facies) metamorphism (M3), the only metamorphic event recorded in the metasedimentary envelope of all the exotic blocks described here.

FORMATION OF 'BLUESCHIST'

The relatively unusual bulk composition of the 'blueschist' sample, given in Table 7, can be explained either by highly fractionated acidic melts of ferrodioritic to plagiogranitic composition, or by extensive metasomatism introducing Na essentially in exchange for Ca. Whilst the surrounding lithology I reflects the 'normal' mineral assemblage as commonly found in metabasalts of the Chameis Complex, lithology II ('blueschist') is almost devoid of Ca, enriched in Na, and shows a rather unusual paragenesis (e.g. lacking any Ca-bearing silicate).

A high degree of freedom of the mineral assemblage containing magnesio-riebeckite does not allow a precise estimation of P–T conditions. None of the existing geothermobarometers can be applied to the observed paragenesis and much depends upon the reaction that is assumed to have produced magnesio-riebeckite in this 'blueschist'. None of the reactions forming this mineral usually found in rocks of basaltic composition (Maruyama *et al.*, 1986) can be applied to lithology II because of the absence of epidote/clinozoisite in the product paragenesis. Textural evidence suggests that magnetite and albite are reactants. Assuming a starting material similar to that encountered in the enclosing metabasalt, and a closed-system behaviour with respect to the non-volatile species, the following reaction might come closest to the true magnesio-riebeckite-forming reaction:

24 edenite + 16 albite + 15 magnetite
+ 48 CO_3 + 56 H_2O = 20 magnesio-riebeckite
+ 15 clinochlore + 48 calcite + 11 quartz.

Magnesio-riebeckite would be a solid solution with 25% ferro-glaucophane component (see Fig. 5). Deviation from

Table 7. Whole-rock X-ray fluorescence analysis of 'blueschist' sample CHB07 from Bogenfels.

		CIPM norms		REE (ppm)	
SiO_2	69.05	Qz	18.8	Sc	13
TiO_2	0.58	Or	0.7	Ba	12
Al_2O_3	11.12	Pl Ab	56.5	Mo	1
Fe_2O_3	1.23	An	0.0	Zr	207
FeO	6.15	Ac	3.6	Y	25
MnO	0.02	Ns	2.4	Sr	20
MgO	1.95	Wo	0.5	U	2
CaO	0.43	Di En	0.2	Rb	4
Na_2O	8.37	Fs	0.3	Th	12
K_2O	0.12	Hy En	4.7	Pb	n.d.
P_2O_5	0.16	Fs	10.0	Zn	7
H_2O^-	0.02	Il	1.1	Cu	3
H_2O^+	—	Ap	0.4	Ni	51
CO_2	—	Total	99.2	Co	18
LOI	1.43			Nb	21
				Cr	48
Total	100.63			V	61
				La	26
				Ce	57
				Nd	29

Values shown have been calculated using oxidation ratio for iron of $Fe_2O_3/FeO = 0.2$.

ideal edenite as a reactant does not significantly affect the phases involved but changes their relative proportions. Using the thermodynamic data set and THERMOCALC program of Powell & Holland (1988), the position of the univariant curve in P–T space for such a magnesio-riebeckite-forming reaction was calculated (Fig. 13). The steep slope of this reaction curve in Fig. 13 does not allow any estimation of pressure. A considerable error in P–T estimates is implied with the discrepancy between the position of the reaction curves as calculated using Powell & Holland's (1988) thermodynamic data set and the experimentally determined curves of Maruyama *et al.* (1986), as shown in Fig. 13. Nevertheless, formation of magnesio-riebeckite within an otherwise 'normal' metabasalt is the presence of some CO_2. Although the modal greenschist facies conditions. The crucial prerequisite for stabilization of the observed assemblage containing magnesio-riebeckite within an otherwise 'normal' metabasalt is the presence of some CO_2. Although the modal proportions of the phases found in the sample are not in perfect accordance with the suggested reaction (particularly the calcite and chlorite contents are too low), indicating an open-system behaviour, the exotic block of 'blueschist' within a polymetamorphic metabasalt of greenschist facies can be attributed to local increased f_{CO_2}. The influence of X_{CO_2} on the equilibrium temperature is however only minor as shown in Fig. 14. In addition, the fluid involved can be characterized by a relatively high f_{O_2} as indicated by the oxidation of magnetite to hematite and the stabilization of magnesio-riebeckite (Okay, 1980) in the 'blueschist' zone. The fluid composition within the 'blueschist' therefore differs strongly from that in the surrounding metabasalt where the alteration of ilmenite to titanite (leucoxene) indicates low X_{CO_2} (Ernst, 1972).

Finally, formation of magnesio-riebeckite at high pressures (>4 kbar) can be excluded for the following reason. If it were a high-P product, some magnesio-riebeckite or, at higher pressure glaucophane, should also be expected in the surrounding metabasalt, together with epidote/clinozoisite and chlorite, which is not the case.

If the Na-rich bulk composition of the 'blueschist' block is caused by metasomatism, the albitization is either related to interaction between seawater and ocean floor, or associated with some later infiltration event. Constraints on the relative timing of the suggested magnesio-riebeckite-forming reaction are given on the one hand by the undeformed state of the albite/quartz veins overgrown by magnesio-riebeckite, and on the other hand by the progressive alignment of these amphiboles close to the highly foliated metabasaltic surrounding. A syntectonic (with respect to obduction of the oceanic crustal rocks) origin of this event is inferred from the textural relationships whereby the unstrained core of the 'blueschist' block is regarded as a more competent and hence strain-protected zone. The high gradient in fluid composition between 'blueschist' and metabasaltic envelope during this event remains problematic. It could be related to local metasomatic calcitization at some earlier

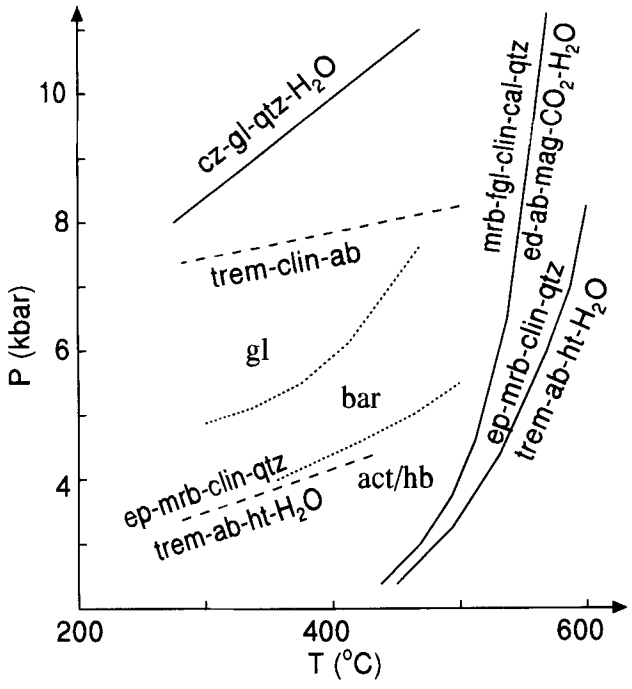

Fig. 13. P–T diagram comparing the stabilities of glaucophane (gl)- and magnesio-riebeckite (mrb)-bearing assemblages. Solid lines = calculated by the program THERMOCALC (Powell & Holland, 1988); dashed lines = experimentally derived curves from Maruyama *et al.* (1986); dotted lines delineate stability fields of glaucophane, barroisite (bar) and actinolite (act)/hornblende (hb) after Ernst (1979); cal = calcite, clin = clinochlore, fgl = ferro-glaucophane, ht = hematite; for other abbreviations see Fig. 12.

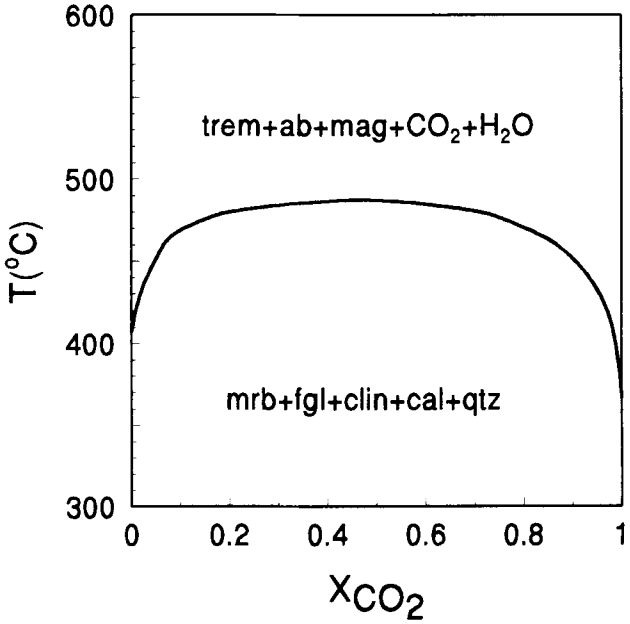

Fig. 14. Isobaric T–X_{CO_2} diagram (P = 4 kbar) for the reaction mrb + fgl + clin + cal + qtz = trem + ab + mag + CO_2 + H_2O as calculated by THERMOCALC (Powell & Holland, 1988); for abbreviations see Figs 12 & 13.

stage with subsequent decarbonation and loss of Ca^{2+} during M2 whereby X_{CO_2} was buffered mainly internally, or to local CO_2-influx derived from a major thrust plane nearby, the basal tectonic contact of the Chameis thrust sheet.

CONCLUSIONS

In contrast to previous descriptions, no evidence for glaucophane or blueschist facies metamorphism could be found in metabasic rocks of the Gariep belt. Hence the most compelling argument for modern Wilson-cycle tectonics triggering blueschist facies metamorphism during Pan-African orogeny in the Gariep belt (Porada, 1989) must be considered to be invalidated. Blue sodic amphiboles recorded previously by Kaiser (1926) and Kröner (1974) are magnesio-riebeckite whose formation can be attributed to retrograde alteration of metabasalt at upper greenschist facies conditions. Blue-green amphiboles in metabasalts, previously described as 'glaucophanitic hornblende' by Kaiser (1926), are of variable edenitic–pargasitic to barroisitic composition. Chemical zonation and textural relationships indicate a three-phase metamorphic history (Fig. 15):

(M1) pre-tectonic replacement of magmatic clinopyroxene by edenitic Amph I at very low pressures and low to medium grade is attributed to hydrothermal sea-floor metamorphism;

(M2) increased crossite content in syntectonic barroisitic Amph II reflects an increase in the P/T ratio to a geothermal gradient of about $30°C\,km^{-1}$ at upper greenschist/amphibolite facies conditions;

(M3) late- to post-tectonic partial replacement of the aluminous amphiboles by actinolite or chlorite is related to regional low-grade (lower greenschist facies) metamorphism.

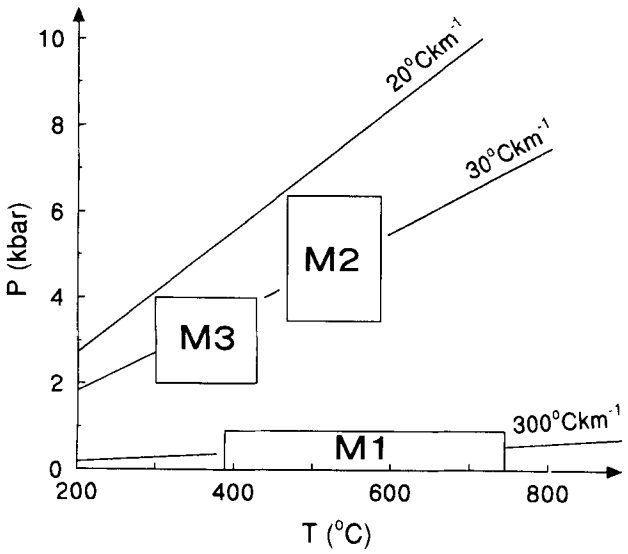

Fig. 15. Approximate P–T conditions during M1, M2 and M3, experienced by the exotic mafic blocks in the Chameis terrane, and inferred from mineral parageneses and amphibole compositions. M1 is considered a sea-floor metamorphic event, M2 is related to a subduction process whilst M3 reflects regional metamorphism, the only event recorded as prograde metamorphism in the sedimentary envelope.

M3 is the only metamorphic event recorded in the sedimentary envelope of the exotic igneous blocks within the tectonic melange zone of the Chameis Complex. Consequently, the mafic rocks that have experienced a higher metamorphic grade than their sedimentary envelope prior to regional metamorphism must have been buried to deeper crustal levels (15–20 km). M2, documented by a more or less adiabatic increase in pressure, could therefore be explained by a subduction-related process that affected only the mafics and ultramafics which were subsequently obducted and tectonically emplaced as exotic blocks into the sedimentary country rocks which in turn were affected only by regional lower greenschist facies metamorphism (M3).

The subduction process that the mafics and ultramafics in the Chameis Complex might have experienced differs from modern ones by having a higher geothermal gradient (see P–T path in Fig. 15). This can hardly be explained by a generally higher heat flow at Pan-Gondwana times in view of true blueschist assemblages described from other late Precambrian terranes (Nakajima *et al.*, 1990), Pan-African eclogites (Vrana *et al.*, 1975; Menot & Seddoh, 1985; Sautter, 1985) and evidence of a Wilson cycle in Pan-African mobile belts (Black *et al.*, 1979). A more likely explanation for the thermal structure of the Marmora Terrane may be either subduction of very young oceanic crust, or a very slow subduction rate operative over only a relatively short period of time, thus not allowing for deep burial of the oceanic crustal slab.

ACKNOWLEDGEMENTS

This research was supported by the University of Cape Town and a Foundation for Research Development grant to H.E.F. C.J.H.H. thanks CDM Namibia, K. Whitelock and K. R. Hazell for permission to enter the Diamond Area in Namibia, I. G. D. Ransome, M. A. Zingg and R. Liddle for assistance in collecting samples. H.E.F. thanks R. S. Richard for his assistance with the electron microprobe. S. Maruyama, D. Robinson and an anonymous reviewer are acknowledged for their constructive comments on the manuscript.

REFERENCES

Afifi, A. M. & Essene, E. J., 1988. *Minfile User Manual, Version 3-88.* Department of Geological Sciences, University of Michigan, 22 pp.

Allsopp, H. L., Köstlin, E. O., Welke, H. J., Burger, A. J., Kröner, A. & Blignault, H. J., 1979. Rb–Sr and U–Pb geochronology of late Precambrian–Early Palaeozoic igneous activity in the Richtersveld (South Africa) and southern South West Africa. *Transactions of the Geological Society of South Africa,* **82,** 185–204.

Apted, M. J. & Liou, J. G., 1983. Phase relations among

greenschist, epidote-amphibolite, and amphibolite in a basaltic system. *American Journal of Science*, **283-A,** 328–354.

Barnes, S. J. & Sawyer, E. W., 1980. An alternative model for the Damara Mobile Belt: ocean crust, subduction and continental convergence. *Precambrian Research*, **13,** 297–336.

Black, R., Caby, R., Moussine-Pouchkine, A., Bayer, R., Bertrand, J. M., Boullier, A. M., Fabre, J. & Lesquer, A., 1979. Evidence for late Precambrian plate tectonics in West Africa. *Nature*, **278,** 223–227.

Blundy, J. D. & Holland, T. J. B., 1990. Calcic amphibole equilibria and a new amphibole–plagioclase geothermometer. *Contributions to Mineralogy and Petrology*, **104,** 208–224.

Brown, E. H., 1977. The crossite content of Ca-amphibole as a guide to pressure of metamorphism. *Journal of Petrology*, **18,** 53–72.

Ernst, W. G., 1972. CO_2-poor composition of the fluid attending Franciscan and Sanbagawa low-grade metamorphism. *Geochemica et Cosmochemica Acta*, **36,** 497–504.

Ernst, W. G., 1979. Coexisting sodic and calcic amphiboles from high-pressure metamorphic belts and the stability of barroisitic amphibole. *Mineralogical Magazine*, **43,** 269–278.

Hartnady, C. J. H., Ransome, I. G. D. & Frimmel, H. E., 1990. Accreted composite terranes—an example from the Gariep orogenic belt. *Abstracts Geocongress '90*, pp. 218–221. Geological Society of South Africa, Cape Town.

Hawthorne, F. C., 1981. Crystal chemistry of the amphiboles: Natural occurrence and theory. In: *Amphiboles and Other Hydrous Pyriboles—Mineralogy, Reviews in Mineralogy*, Vol. 9A (ed. Veblen, D. R.), pp. 1–102. Mineralogical Society of America.

Hekinian, R., 1982. *Petrology of the Ocean Floor*. Elsevier, Amsterdam, 393 pp.

Herbert, R. & Constantin, M., 1991. Petrology of hydrothermal metamorphism of oceanic layer 3: implications for sulfide parageneses and redistribution. *Economic Geology*, **86,** 472–485.

Ito, E. & Anderson, J., 1983. Submarine metamorphism of gabbros from the Mid-Cayman Rise: petrographic and mineralogic constraints on hydrothermal processes at slow-spreading ridges. *Contributions to Mineralogy and Petrology*, **82,** 371–388.

Kaiser, E., 1926. *Die Diamantenwüste Südwestafrikas*. Band I. Dietrich Reimer, Berlin, pp. 190–204.

Kasch, W., 1983a. Regional P–T variation in the Damara orogen with particular reference to early high-pressure metamorphism along the southern margin. *Special Publications of the Geological Society of South Africa*, **11,** 243–253.

Kasch, K. W., 1983b. Continental collision, suture progradation and thermal relaxation: a plate tectonic model for the Damara orogen in central Namibia. *Special Publications of the Geological Society of South Africa*, **11,** 423–429.

Kröner, A., 1974. The Gariep Group I. Late Precambrian formations in the western Richtersveld, Northern Cape Province. *Precambrian Research Unit, University of Cape Town, Bulletin*, **13,** 115 pp.

Kröner, A. & Hawkesworth, C. J., 1976. Late Pan-African emplacement ages for Rössing alaskitic granite (Damara belt) and Rooi Lepel bostonite (Gariep belt) in Namibia and their significance for the timing of metamorphic events. *20th Anniversary Report of the Research Institute for African Geology*, pp. 14–17.

Kröner, A. & Welin, E., 1973. Evidence for a ±500 m.a. old thermal episode in southern South West Africa. *Earth and Planetary Science Letters*, **21,** 149–152.

Laird, J., 1980. Phase equilibria in mafic schists from Vermont. *Journal of Petrology*, **21,** 1–37.

Le Roex, A. P., Erlank, A. J. & Needham, H. D., 1981. Geochemical and mineralogical evidence for the occurrence of at least three distinct magma types in the 'FAMOUS' region. *Contributions to Mineralogy and Petrology*, **77,** 24–37.

Martin, H. & Porada, H., 1977. The intracratonic branch of the Damara orogen in South West Africa. Part I. Discussion of geodynamic models. *Precambrian Research*, **5,** 311–338.

Maruyama, S., Cho, M. & Liou, J. G., 1986. Experimental investigations of blueschist–greenschist transition equilibria: pressure dependence of Al_2O_3 contents in sodic amphiboles—A new geobarometer. In: *Blueschists and Eclogites* (eds Evans, B. W. & Brown, E. H.), *Geological Society of America, Memoirs*, **164,** 1–16.

Menot, R. P. & Seddoh, K. F., 1985. The eclogites of the Lato Hills, South Togo, West Africa: relics from the early teconometamorphic evolution of the Pan-African orogeny. *Chemical Geology*, **50,** 313–330.

Miller, R. McG., 1983. The Pan-African Damara orogen of South West Africa/Namibia. *Special Publications of the Geological Society of South Africa*, **11,** 431–515.

Moody, J. B., Meyer, D. & Jenkins, J. E., 1983. Experimental characterization of the greenschist/amphibolite boundary in mafic systems. *American Journal of Science*, **283,** 48–92.

Nakajima, T., Maruyama, S., Uchiumi, S., Liou, J. G., Wang, X., Xiao, X. & Graham, S. A., 1990. Evidence for late Proterozoic subduction from 700-Myr-old blueschists in China. *Nature*, **346,** 263–265.

Okay, A. I., 1980. Sodic amphiboles as oxygen fugacity indicators in metamorphism. *Journal of Geology*, **88,** 225–232.

Onstott, T. C., Hargraves, R. B. & Reid, D. L., 1986. Constraints on the tectonic evolution of the Namaqua Province III: palaeomagnetic and $^{40}Ar/^{39}Ar$ results from the Gannakouriep dyke swarm. *Transactions of the Geological Society of South Africa*, **89,** 171–183.

Porada, H., 1979. The Damara-Ribeira orogen of the Pan-African/Brasiliano cycle in Namibia (South West Africa) and Brazil as interpreted in terms of continental collision. *Tectonophysics*, **57,** 237–265.

Porada, H., 1983. Geodynamic model for the geosynclinal development of the Damara orogen, Namibia/South West Africa. In: *Intracontinental Fold Belts* (eds Martin, H. & Eder, F. W.), pp. 503–542. Springer-Verlag, Berlin.

Porada, H., 1989. Pan-African rifting and orogenesis in southern to equatorial Africa and eastern Brazil. *Precambrian Research*, **44,** 103–136.

Powell, R. & Holland, T. J. B., 1988. An internally consistent dataset with uncertainties and correlations: 3. Applications to geobarometry, worked examples and a computer program. *Journal of Metamorphic Geology*, **6,** 173–204.

Reid, D. L., Ransome, I. G. D., Onstott, T. C. & Adams, C. J., 1992. Late Precambrian mafic dykes in the lower Orange river region, Southern Africa: possible Constraints on the age of the Precambrian–Cambrian boundary. *Journal of African Earth Science*, in press.

Robinson, P., Spear, F. S., Schumacher, J. C., Laird, J., Klein, C., Evans, B. W. & Doolan, B. L., 1982. Phase relations of metamorphic amphiboles: natural occurrence and theory. In: *Amphiboles, Reviews in Mineralogy*, Vol. 9B (eds Veblen, D. R. & Ribbe, P. H.), pp. 1–65. Mineralogical Society of America.

Sautter, V., 1985. An eclogite paragenesis from the Aleksod basement, Central Hoggar, South Algeria. *Chemical Geology*, **50,** 331–347.

Sivell, W. J. & Waterhouse, J. B., 1984. Oceanic ridge metamorphism of the Patuki Volcanics, D'Urville Island, New Zealand. *Lithos*, **17,** 19–36.

Smith, H. S. & Hartnady, C. J. H., 1984. Geochemistry of Grootderm Formation lavas: indication of tectonic environment of extrusion. *Abstracts, Conference on Middle to Late Proterozoic Lithosphere Evolution*, pp. 20–21.

Spear, F. S. 1981. An experimental study of hornblende stability and compositional variability in amphibolite. *American Journal of Science*, **281,** 697–734.

Vrana, S., Prasad, R. & Fediukova, E., 1975. Metamorphic kyanite eclogite in the Lufilian Arc of Zambia. *Contributions to Mineralogy and Petrology*, **51,** 139–160.

Received 24 July 1991; revision accepted 5 December 1991.